# A pair of NLRs coordinately modulates NRC3-mediated ETI responses to facilitate age-dependent immunity

Xiaohua Dong, Xiaoyan Zhang, Zhiyuan Yin, Jialu Li, Chuyan Xia, Weiye Pan, Yaning Zhao, Maofeng Jing, Jinding Liu, Gan Ai*, Daolong Dou*

[1] College of Plant Protection, Academy for Advanced Interdisciplinary Studies, Nanjing Agricultural University, Nanjing 210095, China

* Corresponding author: Daolong Dou, Email: ddou@njau.edu.cn, Gan Ai, Email: Ganai@njau.edu.cn

**Running title: Paired NLRs regulate age-dependent immunity**

**Email addresses:**

Xiaohua Dong, 2019202017@njau.edu.cn
Xiaoyan Zhang, 12119419@njau.edu.cn
Zhiyuan Yin, zyin@njau.edu.cn
Jialu Li, a13770938276@163.com
Chuyan Xia, chuyan79@icloud.com
Weiye Pan, 12117232@njau.edu.cn
Yaning Zhao, 2018116107@njau.edu.cn
Maofeng Jing, jingmf@njau.edu.cn
Jinding Liu, liujd@njau.edu.cn
Gan Ai, Ganai@njau.edu.cn
Daolong Dou, ddou@njau.edu.cn

# Abstract

Two NLRs (Nucleotide-binding and Leucine-rich repeat Receptors) adjacent to each other on a locus, termed as paired NLRs, may act separately for effector recognition and subsequent signaling activation to mediate effector-triggered immunity (ETI) in many plants. However, it is largely unknown about their distribution and functions in Solanaceae species, in which NLR-Hs (Helpers NLR REQUIRED FOR CELL DEATHs) have been extensively studied. Here, we identified paired NLRs in Solanaceae species and found they harbor paired NLRs ranging from 6 to 100, which are significantly negatively correlated with the numbers of NLR-Hs. *N. benthamiana* has six paired NLRs, among which silencing of *NRCX* exhibits phenotypes of dwarfism and accelerated senescence. Importantly, *NRCX*-silencing phenotypes could be restored by simultaneously silencing its head-to-head NLR pair, thus we named it as *NRCY*. NRCX/Y pair is specific in Solanaceae species. NRCY contains non-canonical walker B and MHD motifs, but could not induce autoactive cell death in *N. benthamiana*. Instead of that, silencing *NRCY* impaired cell death triggered by Sw5b-Nsm and NRC3$^{D480V}$, indicating NRCY is also an NLR modulator like NRCX. Furthermore, NRCX suppression of Sw5b-Nsm and NRC3-mediated cell death is dependent on NRCY. Remarkably, we found that *NRCX* and *NRCY* expressions were induced during plant senescence, while *NRCY* was induced more than *NRCX*. Accordingly, the plant resistance was stronger during maturation, indicated NRCX/Y might be involved in age-dependent resistance. Our study reveals one of the paired NLRs coordinately regulates ETI to facilitate age-dependent immunity.


**Key words:** Paired NLR; NRC helpers; NLR modulator; Age-dependent immunity

# Introduction

Plants have evolved a sophisticated innate immune system to prevent infection from diverse pathogens. PRRs in the cell surface trigger plant immunity by recognizing conserved components of pathogens and hosts, known as the pattern-triggered Immunity (PTI). Successfully adapted pathogens deliver effectors to suppress defense responses including PTI. As a countermeasure, plants have evolved a second layer of immunity involving NLRs (Nucleotide-binding and Leucine-rich repeat Receptors), which recognizes pathogen effectors and trigger effector-triggered Immunity (ETI) [1,2]. ETI provides robust defense responses that are usually associated with cell death, which is referred to be hypersensitive response (HR), at infection sites to inhibit pathogen infection [3,4].

NLRs can function in pairs [5,6]. Paired NLRs are usually genetically adjacent to each other in a 'head-to-head' fashion and physically interact with each other [7,8]. For example, RGA4/RGA5 of rice locates in one locus in a 'head-to-head' form, and they physically interact with each other through CC domain regardless of the presence of effectors [9]. Usually, one of an NLR pair is a sensor, which is specialized to recognize the pathogen and the other is involved in initiating immune signaling (executor) [10]. Most executors are auto-activated and overexpression of these executors causes autoactive cell death *in planta* [10]. The autoactivity of executors can be suppressed by their sensors and knocking-out sensors may lead to lesion mimic phenotypes in plants [11,12]. The downstream signaling pathway of NLR pairs partially involves helper NLRs (NLR-Hs), e.g. ADR1 and NRG1 [13], which may form $Ca^{2+}$-permeable cation channels to directly regulate cytoplasmic $Ca^{2+}$ levels and consequent cell death [14].

NLRs work not only in pairs, but also through a complex network architecture [15]. Recently, a major clade of NLRs in Solanaceae plant species was shown to form a comprehensive network. In this network, multiple helper NLRs, known as NLR-Hs (Helpers NLR REQUIRED FOR CELL DEATHs), are required by a large number of sensor NLRs that mediate resistance against

diverse pathogens [16]. For example, Sw5b, an NLR from *Solanum lycopersicum*, could recognize Nsm from Tospoviruses and trigger a NRC2/3-dependent HR [16,17]. Unlike typical paired NLRs, NRC-Hs are not always clustered with sensor NLRs in plant genomes even though they are evolutionarily related [16]. The current evolutionary model for the NRC network is that it has evolved from a few genetically linked NLRs, as in the Caryophyllales, through a massive expansion of sensors and a relatively limited expansion of helpers, possibly to maintain the robustness of the network against rapidly evolving pathogens [6,18].

NLRs share a basic protein architecture consisting of a variable N-terminal domain, a central nucleotide-binding domain (NB-ARC), and a C-terminal leucine-rich repeat domain (LRR) [19]. NB-ARC domains can be subdivided into three subdomains: NB, ARC1 and ARC2 [19,20]. The NB subdomain contains two major motifs, a P-loop motif required for nucleotide binding and Walker B required for adenosine triphosphate (ATP) hydrolysis [21]. In addition, there is also a nucleotide binding site MHD (methionine-histidine-aspartate) motif on ARC2 [22]. Mutation in the NLR Walker B motif or MHD motif often leads it to be auto-activated [23]. For example, the substitution of the conserved second aspartate to glutamate will reduce ATP hydrolysis rates of I-2 and lead it to autoactivation. Notably, the MHD motifs of many executor NLRs are non-canonical, and are required for auto-activation [23]. For example, the MHD motif of RGA4 is “TYG”, which is highly degenerated, differs from the consensus MHD sequence. Changing the degenerated motif to canonical MHD motif impairs the RGA4 autoactivity [9].

Age-dependent immunity is referred to the phenomenon that plant resistance to pathogens gradually increases with plant age [24]. Age-dependent immunity extensively exists in different plants. For example, *N. benthamiana* has age-dependent resistance against *P. infestans*, by which 35 days old plants have performed a completely resistance to *P. infestans* [25]. Recently, many molecular mechanisms behind age-dependent immunity have

been discovered. In *N. tobaccum*, NLRs and sRNAs are reported to be associated with age-dependent immunity. During the maturation process of plants, NLRs expressions are increasing while small RNAs (sRNAs), which served as the regulatory of NLRs, are gradually decreasing in the expression [26]. The works provide a glimpse into mechanisms behind age-dependent immunity. However, other genes involved in age-dependent immunity are largely unknown.

It is proposed that functional specialization is a critical strategy in NLR evolution to avoid being constrained by signaling activity during evolution [6]. NLR networks built by helper NLR, as well as paired NLRs, require more than one NLR to mediate immune activity. We suspected that there may be redundancy between the functions of paired NLRs and helper NLRs. In this study, by analyzing the distribution of paired NLRs in Solanaceae species, we found that the quantities of paired NLRs and NRC-Hs are negatively correlated. We further used *N. benthamiana*, a model plant of Solanaceae, to evaluate the paired NLRs functions. We found that *N. benthamiana* exhibited significant dwarfing and senescence phenotypes when one of the six paired NLRs, *NRCX*, was silenced. *N. benthamiana* knockout mutant *nrcx* confirmed that the defense responses of *nrcx* are continuously activated. Interestingly, silencing the head-to-head NLR of *NRCX*, *NRCY*, could restore the stunting and senescence phenotype. NRCY is not a autoactive NLR but a positive modulator of NRC3-mediated immunity. Finally, we observed a gradual increase in *NRCX*/*NRCY* expressions as the leaves became senescent, where *NRCY* is induced greatly more, implied that they play a role in age-dependent resistance of *N. benthamiana*.

# Results

## The quantities of paired NLRs and NRC-Hs are negatively correlated in Solanaceae species

To evaluate the distribution of paired NLRs and NRC-Hs in Solanaceae species, we first used NLRtracker tool to identify all NLRs in 29 representative plant species including nine Solanaceae species (Fig 1A, S1 Fig). Assembled genome sizes of these organisms ranged from 89 Mb to 2,918 Mb, with annotated protein counts ranging from 23,879 to 69,500 (S2A Fig). In total, we identified 8,795 non-redundant NLR, ranging from 32 to 852 in each species (Fig 1A). The number of NLRs identified in this study is highly similar to the previous publication [27], supporting the robustness of our pipeline (S2B Fig). Paired NLRs in all these species were identified based on searching NLRs in a "head-to-head" fashion with enclosing no more than 2 non-NLR genes (Fig 1A, S1 Fig) [28]. Helper NLRs (NRC-Hs) were identified through phylogenetic assay (Fig S1, S2 File): the NLRs in the same clades with NRC2/3/4 were considered as NRC-Hs [29] (Fig 1A).

We next investigated the correlation between the %Paired NLR and %NRC-Hs through regression analysis. Interestingly, the %Paired NLRs are negatively correlated with the %NRC-Hs in Solanaceae species (Fig 1B). The slope of the linear fitting equation is -0.6485 with a high R square ($R^2$ = 0.7157). Furthermore, Pearson correlation analysis indicated a high negative correlation between %Paired NLR and %NRC-Hs (Pearson's $r$ = -0.84597) in Solanaceae species. In contrast, no correlation between %Paired NLRs and %NRC-Hs could be detected in other tested species ($R^2$ = 0.02493, Pearson's $r$ = -0.15787) (Fig 1B). We also identified NLRs in "head-tail" or "tail-tail" fashion in Solanaceae species and found no correlation between them with NRC-Hs could be detected (S3A and S3B Figs).

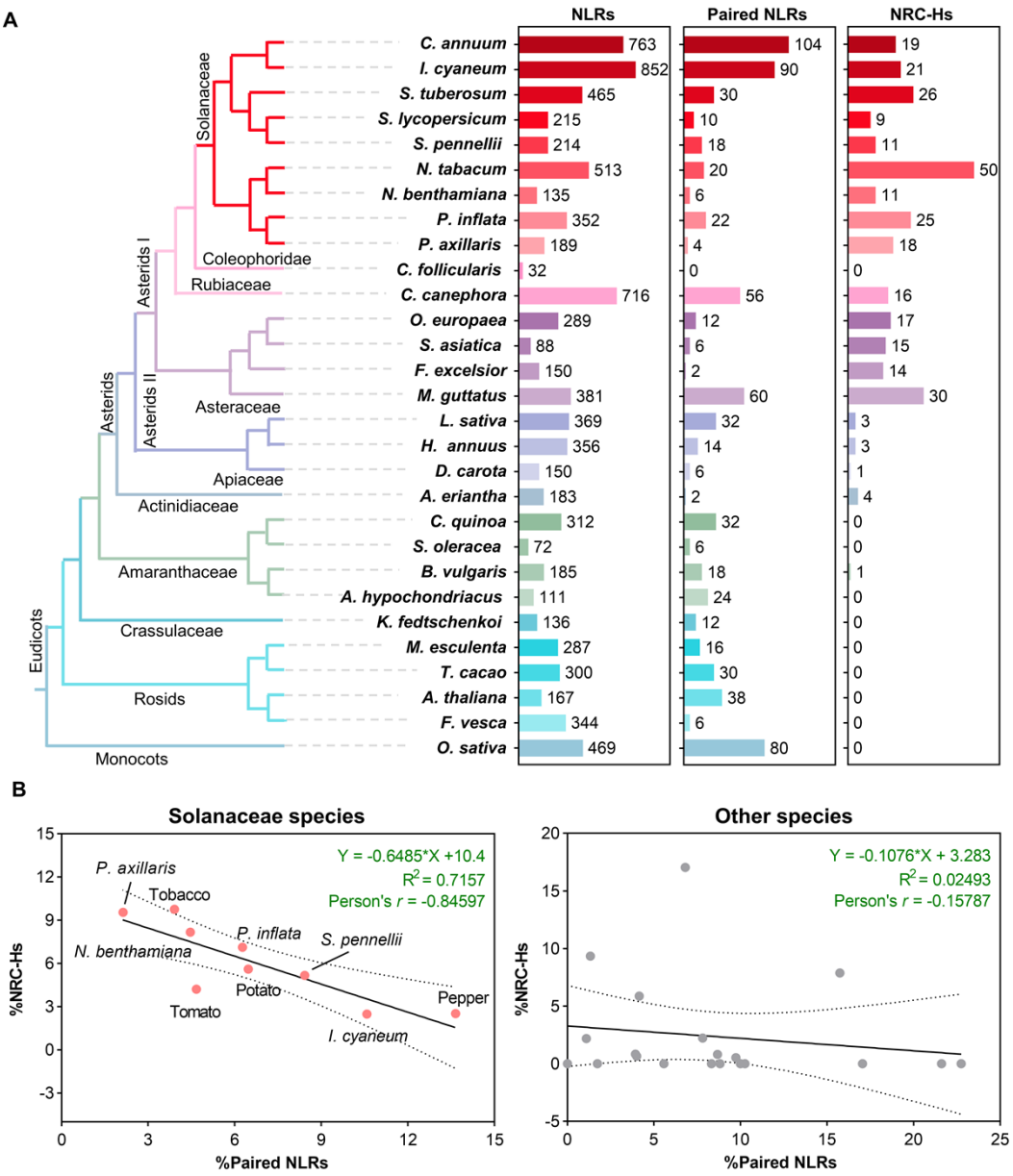


**Fig 1. The quantities of paired NLRs and NRC-Hs are negatively correlated in Solanaceae species**

(A) Summary of predicted NLRs. The phylogeny of the 29 species is based on data from the Taxonomy Database (https://www.ncbi.nlm.nih.gov/taxonomy). The counts of NLRs, paired NLRs and NRCH-s in each species are shown in boxplots following the species names. (B) Scatter plot of %Paired NLRs against %NRC-Hs. Black line represents the linear trend, with dotted line representing the 95% confidence interval. Regression equation (with its R square value) and Person correlation value is shown at top right.

## Silencing *NRCX* leads to a dwarf and accelerated senescence phenotype in *N. benthamiana*

The negative correlation between paired NLRs and NRC-Hs probably resulted

183 from the functional redundancy between them during evolution, which might
184 reduce the selection pressure on paired NLRs and result in loss of function or
185 even novel function. To test it, we used the *N. benthamiana* as a model. The *N.*
186 *benthamiana* only has 6 paired NLRs, which are paired NLR 1a/b (PN1a/b),
187 PN2a/b and PN3a/b (Fig 2A). To evaluate their functions, we silenced all 6
188 paired NLRs individually (Fig 2A). We observed a different phenotype only
189 when *PN3b* was silenced (Fig 2B). qRT-PCR analysis indicated that all the
190 paired NLRs were silenced successfully (S4A Fig).
191 We then focus on the function of PN3b. Further sequence analysis
192 indicated that PN3b is NRCX, an NLR modulator protein negatively regulates
193 NRC2/3-mediated immunity response identified in a parallel research [30]. In
194 addition to a dwarf phenotype (S4B Fig), silencing *NRCX* also made the plant
195 senescence accelerated (S4C and S4D Figs). The tobacco rattle virus
196 accumulation levels in NRCX-silenced plants were lower than those in control
197 lines, indicating that the dwarf phenotype is not resulted from
198 over-accumulated virus (S4E Fig).
199
200 **The senescence-accelerated and dwarf of *nrcx* mutant are spontaneous**
201 To further remove the possibility that such phenotype was caused by the
202 virus or off-target effect of VIGS technology, we used CRISPR/Cas9 system to
203 generate *NRCX* loss-of-function mutants. One small guide RNA (sgRNA) was
204 designed based on the unique sequence of NRCX (Fig 2C) and transformed
205 together with Cas9 and a kanamycin selection maker into *N. benthamiana*.
206 Nine independent transformants were selected using kanamycin. Among the
207 recovered lines, only one transformant containing a 7 bp deletion in the *NRCX*
208 locus was a homozygous *nrcx* mutant (Fig 2C), while the other transformants
209 were heterozygous or wild-type. No off-target effects were found in *NRCX*
210 homologues (S5A and S5B Figs). The development of *nrcx* mutants was
211 significantly arrested compared to that of the wild type (Fig 2D), suggesting
212 that loss-of-function of *NRCX,* rather than the virus and off-target effect of

VIGS technology, was responsible for the phenotypes.

To figure out whether the *nrcx* phenotypes are spontaneous or stimulated by the microbiome in the soil, *nrcx* and wild-type plants were grown in microbiome-free medium (Fig 2E). Compared with wild type, *nrcx* mutants had a high degree of chlorosis and were smaller (Figs 2F-H), indicating that the dwarfing and accelerated aging phenotype of *nrcx* is spontaneous. Importantly, we found that *nrcx* mutants showed higher inhibition levels in the root than in the stem (Figs 2G and 2H), indicating that NRCX plays a vital role in root development, which is consistent with the report that *NRCX* is highly accumulated in roots [30].

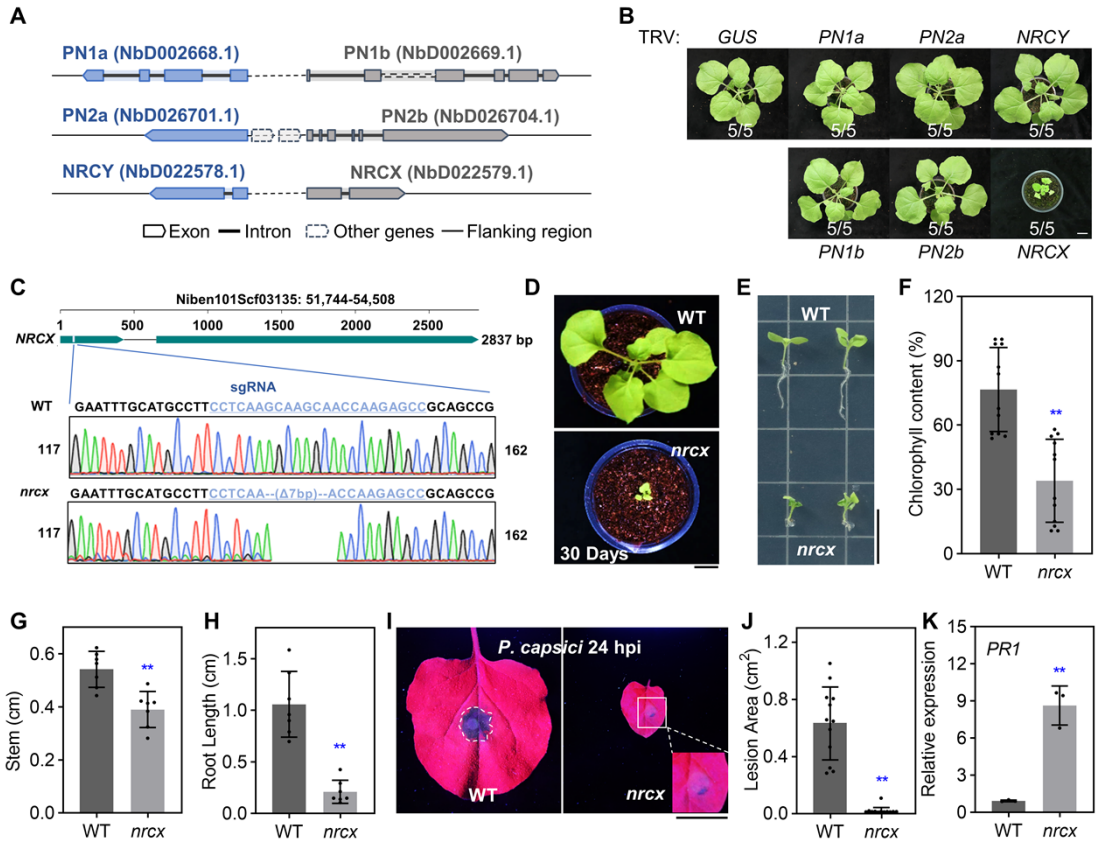


**Fig 2. Mutant of *NRCX* is senescence-accelerated, display growth defect and high resistance level.**

(A) Schematic diagram of six paired NLRs in *N. benthamiana.* (B) The morphology of plants silencing indicated genes. Two-week-old *N. benthamiana* plants were infiltrated with *Agrobacterium* strains carrying tobacco rattle virus (TRV) VIGS constructs, and photographs were taken 4 weeks after agroinfiltration. TRV:*GUS* (*β-glucuronidase*) was used as a negative control. Bar = 2 cm. (C) Schematic diagram showing the deletion of

*NRCX* in *N. benthamiana*. The genomic region information of *NRCX* is shown above. The gRNA used for CRISPR/Cas9 editing and DNA sequencing results are shown below. (D) Phenotypes of wild type and *nrcx* knockout mutants grown in soil for 30 days. Bar = 2 cm. (E) Phenotypes of wild type and *nrcx* mutant seedlings on sterile 1/2 MS medium for three weeks. Bar = 1 cm. (F) Chlorophyll content in leaves of *N. benthamiana* wild type and *nrcx* mutant. Asterisks indicate statistically significant differences with t test (mean ± SD, n = 12, $^{**}P < 0.01$), and asterisk in the following text indicates the same meaning. (G,H) Stem length and root length statistics of wild type and *nrcx* grown on 1/2 MS medium for 3 weeks (mean ± SD, n = 7). (I-J) Enhanced resistance in *nrx* mutant. The photos were taken at 24 hours after inoculation (hpi) under UV light. Bar = 2 Inoculated lesion areas are show in (J) (mean ± SD, n = 12). (K) Upregulation of *PR1* expression in *nrcx* mutant. The indicated leaves were inoculated with *P. capsici* for 12 hours and the *PR1* expression was tested (mean ± SEM, n = 3).

## Defense response is activated in *nrcx* mutant

Plant growth and resistance are often in a state of ebb and flow, the dwarf and accelerated senescence phenotype may result from the persistent activation of plant immunity [31-33]. *Phytophthora* inoculation assay indicated that *nrcx* plants exhibited high levels of resistance to *P. capsici* (Figs 2I and 2J). To test whether the defense response was activated in *nrcx* mutants, the *PR1* (*Pathogenesis-related protein 1*) gene of wild-type and *nrcx* mutants were tested separately, and *PR1* was up-regulated about ~10 fold in *nrcx* mutant plants (Fig 2K). Collectively, these results suggest that defense responses are continuously activated in *nrcx* plants.

## Simultaneously silencing *NRCY* restores the *NRCX*-silenced plants phenotype

Knocking-out one paired NLR may activate their conjugated NLR to activate defense pathways and inhibit plant growth [34]. The head-to-head NLR (*PN3a*) of *NRCX* is named after *NRCY* (*NLR-REQUIRED FOR CELL DEATH Y*) (Fig 2A). *NRCY* and *NRCX* are tandemly linked in a head-to-head manner on a scaffold with an intergenic region of 18,795 bp between them. We assumed that, like other NLR pairs, *NRCX* silencing may activate NRCY and subsequently induce plant defense responses. To verify this, we co-silencing

*NRCX* and *NRCY* in plants using one TRV vector where the gene fragments of *NRCX* and *NRCY* were tandemly cloned. Compared to TRV:*NRCX* plants, growth inhibition and accelerated senescence are significantly restored in TRV:*NRCX/Y* plants, even though TRV:*NRCX/Y* plants were still smaller than TRV:GUS (*β-glucuronidase*) plants (Figs 3A-C). qRT-PCR assays indicated that these genes had been successfully silenced (Figs S6A and S6B).

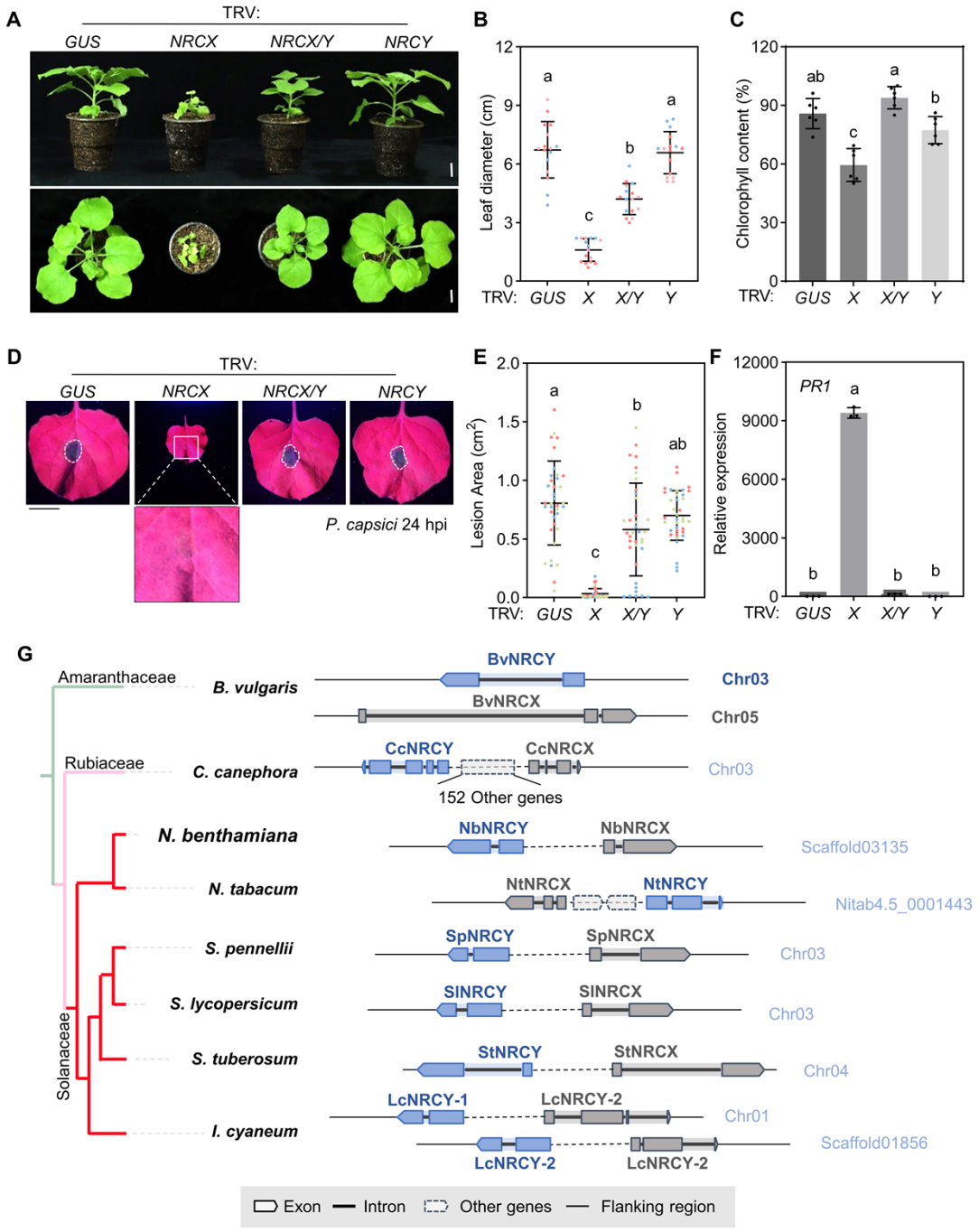


**Fig 3. Simultaneously silencing *NRCY* restores the *NRCX*-silenced plants**

**phenotype.**

(A) The morphology of *N. benthamiana* plants silencing indicated genes. TRV:*GUS* was used as a negative control. Two-week-old *N. benthamiana* plants were infiltrated with *Agrobacterium* strains carrying TRV constructs, and the photographs were taken 4 weeks after agroinfiltration. Bar = 2 cm. (B) Leaf diameter of plants silencing indicated genes. The fourth and fifth true leaves (counting from bottom to top) were harvested and the average diameters were recorded. Three independent biological replicates were performed and indicated by different colored dots (n = 16, lowercase letters indicate significant differences tested between multiple groups by one-way ANOVA at $P < 0.05$). (C) Chlorophyll contents of indicated leaves. The fourth true leaf (counting from bottom to top) was taken from five plants silencing indicated genes at 6 weeks of age and the chlorophyll contents were calculated (n = 6, lowercase letters indicate significant differences tested between multiple groups by one-way ANOVA at $P < 0.05$). (D-E) *P. capsici* inoculation phenotypes. Leaves of plants silencing indicated genes were detached and inoculated with *P. capsici* and then incubated in a growth room at 25°C in darkness. Bar = 2 cm. Lesion area was calculated and is shown at (E). Different colored dots indicate different repetitions (n = 37, lowercase letters indicate significant differences tested between multiple groups by one-way ANOVA at $P < 0.05$). (F) Relative *PR1* gene expression levels. The indicated leaves were inoculated with *P. capsici* for 12 hours and the PR1 expression was tested (mean ± SEM, n = 3). (G) Schematic diagram of NRCX and NRCY plant genomes.

We next tested whether the activated immunity in TRV:*NRCX* plants is impaired in TRV:*NRCX/Y*. The enhanced resistance to *P. capsici* in TRV:*NRCX* plants was partially restored in TRV:*NRCX/Y* (Figs 3D and 3E). Similarly, the *PR1* expressions in *NRCX/Y*-silenced plants were significantly lower than that in TRV:*NRCX* plants (Fig 3F). Collectively, these results indicated that NRCY was a positive regulator of plant immunity and senescence. And the dwarf and accelerated senescence phenotype of *NRCX*-silenced plants is partially dependent on NRCY.

## NRCX/Y pair is specific in Solanaceae species

We further tested whether the NRCX and NRCY conserved. According to our phylogenetic assay (S7 Fig). NRCX homologs could be first discovered in *B. vulgaris* during evolution and are specific in Asterids species, which is consistent with the previous results [30]. Meanwhile, NRCY are conserved in dicots (S7 Fig). We further analyzed the distribution of paired NRCX/Y by

311 analyzing whether they are tandemly located in one locus (no more than 2
312 other genes between them). In *B. vulgaris* (sugar beet), NRCX and NRCY
313 homologs are located in different chromosomes (Fig 3G). In *C. canephora*
314 (coffee), NRCX and NRCY are found in same chromosomes but separated by
315 152 other genes (Fig 3G). In contrast, NRCX/Y are adjacent to each other and
316 conserved in *N. tabacum*, *N. benthamiana*, *S. pennellii*, *S. lycopersicum*, *S.*
317 *tuberosum*, *I. cyaneum*, indicated that the paired NRCX/Y is specifically
318 encoded by Solanaceae species (Fig 3G).
319
320 **The walker B and MHD motifs of NRCY are non-canonical**
321 *NRCY* encoded an 881-aa CNL containing a CC domain, an NB-ARC
322 domain and an LRR domain. P-loop, walker B and MHD motifs within the
323 NB-ARC domain are important for NLR activation and mutations of critical
324 residues in these motifs may lead to NLR autoactivation [23]. Sequence
325 analysis indicated that the P-loop sequence of NRCY matches the consensus
326 sequence (GxxxxGK[T/S]) (Fig 4A). Interestingly, in the walker B motif of
327 NRCY, the conserved second aspartate is naturally substituted by glutamate
328 (Fig 4A), and this mutation was reported to result in reduced ATP hydrolysis
329 rates and autoactivation of I-2 [35]. Furthermore, the MHD motif of NRCY is
330 highly degenerated, with all three amino acids distinct from the consensus
331 MHD sequence (Fig 4A). Similarly, NLRs with the non-canonical MHD motif
332 also frequently induce cell death [23].
333 Phylogenetic assay showed that the walker B motif and MHD motif of all
334 NRCY homologs in Arabidopsis, kiwifruit and sugar beet and are canonical (S7
335 Fig). The non-canonical MHD motif emerged in partially NRCY homologs of
336 coffee, while non-canonical Walker B motif emerged in Solanaceae species
337 (S7 Fig), indicating that these two motifs might degenerate during the NLR
338 evolution in Solanaceae species.
339
340 **NRCY does not induce autoactive cell death in *N. benthamiana***

Based on the non-canonical walker B and MHD motifs in NRCY, it is assumed that NRCY is an automatically activated NLR. Transient expression was performed on *N. benthamiana* to detect whether NRCY was self-activating according to the phenomenon of cell death. Surprisingly, no cell death was detected when expressing *NRCY* in leaves, regardless of whether the protein was fused to a tag (Fig 4B). Western blot analysis indicated that *NRCY* was expressed correctly (Fig 4C).

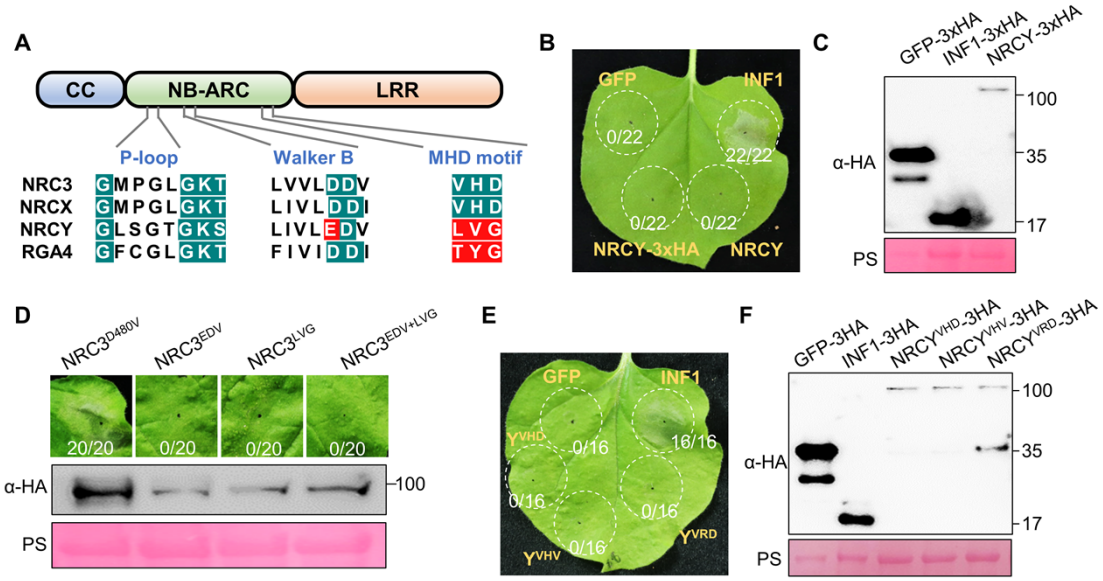


**Fig 4. NRCY does not induce HR in *N. benthamiana*.**
(A) P-loop, walker B and MHD motifs of indicated NLRs. The motif sequences of NRC3, NRCX, NRCY and RGA4 are shown. Canonical residues in motifs are marked by blue while non-canonical residues are marked by red. (B) The phenotype of leaves expressing NRCY. GFP and INF1 were used as negative and positive controls for cell death, respectively. (C) Protein accumulation of NRCY in *N. benthamiana*. Proteins were extracted from leaves at 36 hours after the agroinfiltration. Indicated protein was detected using HA antibody. Total protein loading was confirmed by Ponceau S staining. (D) Cell death induced by the NRC3 mutants. $NRC3^{D480V}$ is an autoactive NRC3 mutant. The phenotypes of leaves expressing NRC3 with walker B motif of NRCY ($NRC3^{EDV}$), NRC3 with MHD motif of NRCY ($NRC3^{LVG}$) and NRC3 with both walker B and MHD motif of NRCY ($NRC3^{EDV+LVG}$) are shown above. Accumulation of the NRC3 variant proteins is shown below. (E) Phenotype of leaves expressing autoactive NRCY mutants. Photos were taken at 5 days post infiltration. (F) Protein accumulation of NRCY autoactive mutants. Total protein loading was confirmed by Ponceau S staining.

These results inspired us to investigate whether the walker B and MHD motifs of NRCY are auto-activated mutants. The original walker B and MHD

motifs of NRC3 were replaced by the walker B and MHD motifs of NRCY. NRC3 with walker B motif of NRCY ($NRC3^{EDV}$), NRC3 with MHD motif of NRCY ($NRC3^{LVG}$) and NRC3 with both walker B and MHD motifs of NRCY ($NRC3^{EDV+LVG}$) induced no cell death when overexpressed in *N. benthamiana*, while $NRC3^{D480V}$ triggered severe cell death (Fig 4D). The protein levels of $NRC3^{EDV}$, $NRC3^{LVG}$ and $NRC3^{EDV+LVG}$ were lower than $NRC3^{D480V}$, but these mutants were expressed correctly (Fig 4D). These results indicated that the walker B and MHD motif of NRCY were not auto-activated mutants. Next, we changed the mutated MHD motif of NRCY to typical auto-activating mutants ($NRCY^{VHV}$ and $NRCY^{VRD}$) and they also triggered no cell death (Figs 4E and 4F). These results suggest that, like NRCX [30], NRCY does not possess the ability to induce cell death.

**Silencing *NRCY* impairs Nsm-Sw5b and NRC3-mediated cell death**

The observation that NRCY is a genetic suppressor of NRCX and is not an auto-activated NLR leads us to ask whether NRCY is another NLR modulator that regulates the function of NRC network. To test this, RNAi technology was used to silence *NRCY* in *N. benthamiana* leaves (S6C Fig), and Sw5b/Nsm, Avr3a/R3a, auto-activating mutants of NRC3 and NRC4 were subsequently expressed. No differences in cell death mediated by NRC4 auto-activating mutants, Avr3a/R3a and INF1 was detected in *NRCY*-silencing leaves (Fig 5A). However, *NRCY*-silencing led to impaired cell death induced by $NRC3^{D480V}$ and Nsm-Sw5b (Figs 5A and 5B), which indicated that NRCY is a positive modulator of NRC3 function.

To characterize the genetic relationship between NRCX and NRCY, *NRCX* and *NRCY* were co-silenced. Although silencing *NRCX* enhanced cell death induced by $NRC3^{D480V}$ and Nsm-Sw5b (S8A-C Figs) [30], co-silencing *NRCX* and *NRCY* still inhibited the cell death, consistent with phenotypes in plants silencing *NRCY* alone (Figs 5C and 5D). These results indicated that the function of NRCX in regulating NRC3 is dependent on NRCY. Collectively,

NRCX/Y are paired NLR modulators that coordinately regulate NRC3-mediated immunity.

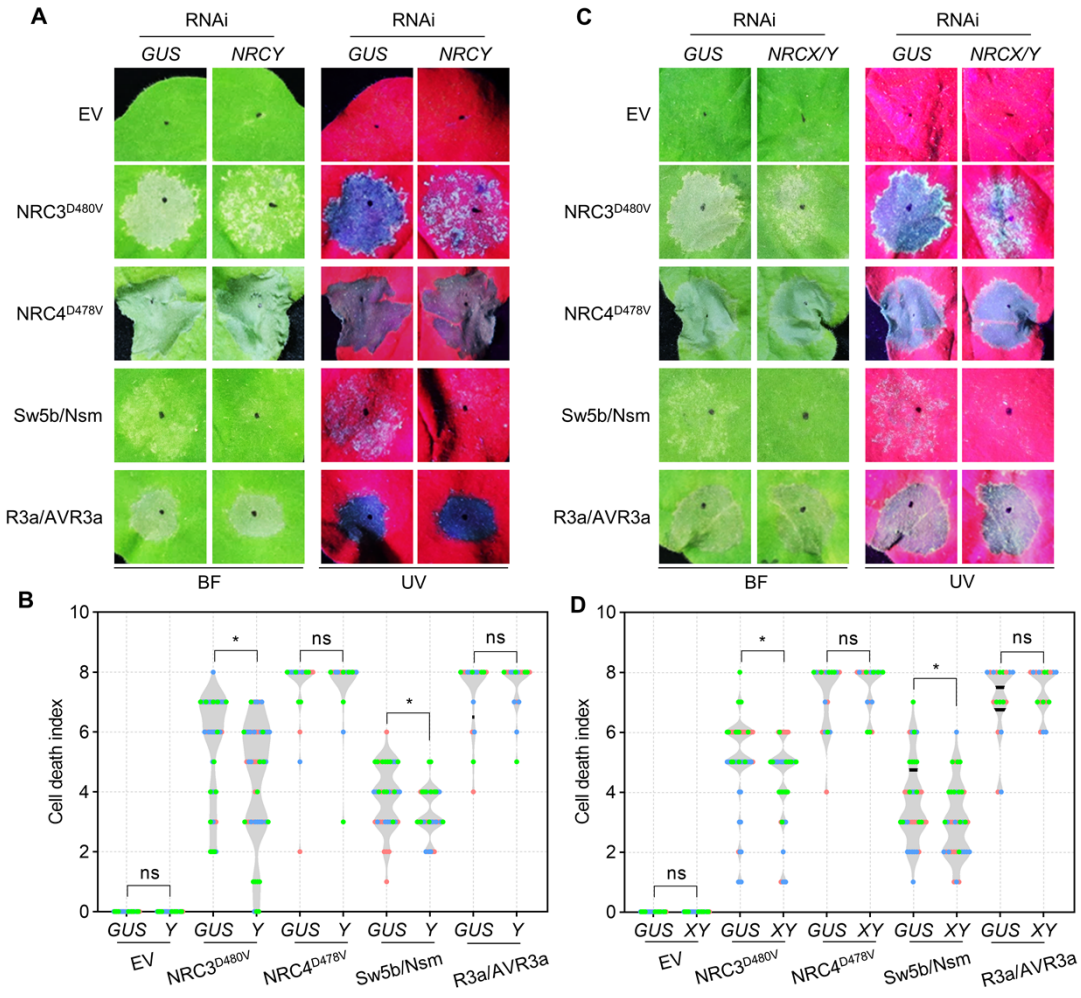


**Fig 5. Silencing NRCY impairs Nsm-Sw5b and NRC3-mediated cell death.**
(A-D) Hypersensitive response phenotypes in indicated leaves. Photos were taken at 5 days post infiltration and are shown (A,C). Violin plots in (B,D) showing the HR index scored at 5 days post agroinfiltration. Three independent biological replicates were performed and indicated by different colored dot. Asterisks indicate statistically significant differences with *t* test (n > 14, $^{**}P < 0.01$).

## Association occurs between CC domains of NRCY and NRCX

Paired NLRs are adjacent to each other at the genome locus and often display physical interactions [6,36]. As our data indicated that NRCX/Y is not a typical NLR pair, it is interesting to test whether there is still a physical interplay between NRCX and NRCY. However, we could not express full-length NRCX protein in *N. benthamiana* correctly, so we did not investigate their association

413 using full length NRCX/Y. Instead of that, we test the association between their
414 domains via split-luciferase assays and yeast two-hybrid (Y2H) (S9A Fig). The
415 results indicated that the CC domains of NRCY and NRCX interact with each
416 other (S9B and S9C Figs).
417
418 **_NRCX_ and _NRCY_ are involved in age-dependent plant immunity**
419 Head-to-head NLR pairs are often transcribed at an equal rate to prevent
420 autoimmune triggered by the executors. As NRCX/Y are NLR modulators, we
421 asked whether the transcriptions of *NRCX* and *NRCY* are still synchronous.
422 Interestingly, when we analyzed the expression of *NRCX* and *NRCY* during
423 leaf senescence, we found that, although the expression of *NRCX* and *NRCY*
424 increased gradually during leaf senescence, their growth rates were different
425 (Figs 7A and 7B). *NRCX* was up-regulated 5-fold in mature leaves compared
426 to young leaves, whereas *NRCY* induced ~30-fold change (Figs 7A and 7B).
427 Age-dependent immunity is referred to the phenomenon that the plant
428 resistance to pathogens is gradually increases during plant maturation [24].
429 We tested the resistance of senescent leaves and young leaves to *P. capsici*,
430 and found the resistance increased gradually (Figs 7C-E). The high growth
431 rate of *NRCY* expression level and the relatively low growth rate of *NRCX*
432 expression level during leaf senescence indicated that the paired NLR
433 modulators may be involved in age-dependent immunity (Fig 7F).
434

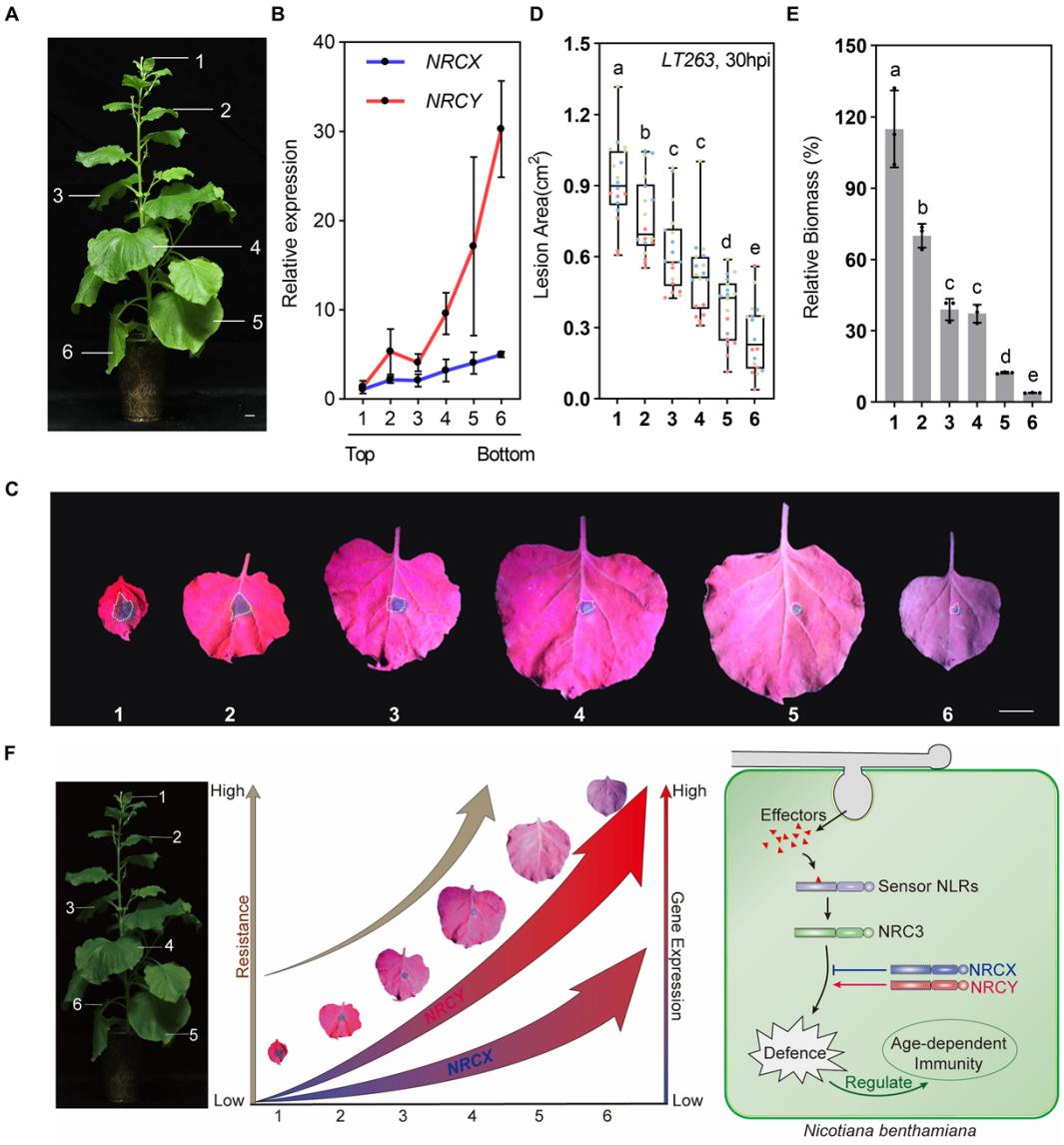


**Figure 7. *NRCX* and *NRCY* are involved in age-dependent plant immunity.**

**(A,B) Upregulation of *NRCX* and *NRCY* during leaf senescence.** Leaf positions used to evaluate *NRCX/Y* expressions are labelled in (A). A total of 6 leaves in each positions were sampled for qRT-PCR assay. The relative expression levels of *NRCX* and *NRCY* in leave 1-6 are shown in (B) (mean ± SEM, n = 3). Bar = 2 cm **(C-E) Age-dependent immunity of *N. benthamiana to P. capsici*.** Leaves from positions indicated in (A) were sample and inoculated with *P. capsici* mycelium. The photos were taken at 24 hpi (C). Lesion areas were calculated and are shown in (D). Three independent replicates were performed and labelled by different colors (mean ± SD, n > 15, lowercase letters indicate significant differences tested between multiple groups by one-way ANOVA at $P < 0.05$). Relative biomass of *P. capsici* is shown in (E) (mean ± SEM, n = 3, lowercase letters indicate significant differences tested between multiple groups by one-way ANOVA at $P < 0.05$). (F) illustration of working model. The paired NLRs, NRCX/Y, coordinately modulate NRC3-dependent immunity and are involved in age-dependent immunity through different expression level during leave maturation.

# Discussion

We identified the paired NLRs and NRC-Hs in the representative Solanaceae species and found a negative correlation between their numbers, suggestive of their potential redundant functions. Using a knock-down assay, we found that *NRCX*-silenced *N. benthamiana* lines exhibited obvious dwarfism and accelerated senescence, which could be restored when its head-to-head NLR pair, *NRCY*, was silenced. Furthermore, we demonstrated that *NRCX* and *NRCY* differently modulates NRC3-mediated immunity, thereby coordinately regulating ETI response in *N. benthamiana*. Finally, we found that *NRCX* and *NRCY* were up-regulated during plant senescence, while the expression of *NRCY* was induced more than *NRCX*. Accordingly, plant resistance was getting stronger throughout maturation, indicating NRCX/Y might be involved in age-dependent resistance. Collectively, we propose that the paired NLRs, NRCX/Y, are novel modulators in age-dependent immunity by coordinately regulating NRC3-mediated immunity (Fig 7F).

Functional specialization is a vital event in NLR evolution that enhances NLRs capacity to keep up with rapidly evolving pathogens without being constrained by signaling activity [6]. In Solanaceae species, NRC-Hs and their sensors expanded greatly [16]. The putative redundant function of NRC-Hs and paired NLRs might reduce the selection pressure of paired NLRs. In this study, we identified the paired NLRs in Solanaceae species and found a high negative correlation between paired NLRs and NRC-Hs. Further silencing experiments showed that, unlike a parallel work in rice, when one of the putative NLR pairs was knocked out, the lesion-mimicking or dwarfing phenotype was widespread [28]. Moreover, we found that *N. benthamiana* exhibited significant dwarfing and senescence phenotypes only if *NRCX* was silenced, which is consistent with the previously study [30]. Furthermore, although NRCX/Y contain many feathers of typical paired NLR, they are NLR

480 modulators. These results might indicate that paired NLRs have degenerated
481 during NRC-Hs expansion in Solanaceae species. Interestingly, in pepper and
482 lochroma, the situation is reversed: %NRC-Hs is relative fewer and
483 the %paired NLRs are large in number, indicated that NLR pairs still function
484 majorly in ETI in the two species.

485 Paired NLRs work together to regulate immunity and usually play different
486 functions. One of them specifically recognizes effectors through specific
487 domains such as HAM (Heavy-Metal Associated domain) and WRKY, and the
488 other activates immune response including cell death [37-40]. However, the
489 NLR pair NRCX/Y found in this study acts more like immune modulators.
490 Neither NRCX nor NRCY has obtained an integrated domain that can
491 recognize effector structures like HAM and WRKY domain. Moreover, multiple
492 putative activating mutants of NRCX and NRCY could not induce the HR
493 response of *N. benthamiana* [30], indicating that the mode of action of NRCX
494 and NRCY is different from the traditionally considered paired NLRs. Instead of
495 that, the NRCX/Y modulate NRC3-dependent immunity. On the other hand,
496 NRCX/Y still maintain some typical feathers of NLR pair. Firstly, they located in
497 genome in a “head-to-head” fashion. Secondly, knocking out *NRCX* did induce
498 a dwarf phenotype, which is reminiscent of knocking out sensor NLR in a
499 typical NLR pair. Thirdly, paired NLRs usually interact with each other [9,40,41],
500 and we found their CC domains can form heterodimer. These indicated that
501 the NRCX/Y pair might be in a transitional stage with both original and novel
502 feathers.

503 The NB-ARC domain of NLRs acts as a molecular switch for ATP
504 hydrolysis, switching from the ‘off’ state of ADP binding to the ‘on’ state of
505 ATP-binding to activate downstream immune responses [21,42]. The walker B
506 motif (hhhDD/E) and MHD motif motifs are important for ATP hydrolysis and
507 ADP binding, respectively [22,43,44]. Mutation in the two motifs often results in
508 an autoactive phenotypes [45]. Although NRCY has a non-canonical walker B
509 (LIVLEDV) and MHD motif (LVG), it cannot induce cell death. The results

510 further supported that NRCY is more of a modulator than an executor.
511 Interestingly, we found the non-canonical motifs of NRCY emerged in coffee,
512 which is closely to the emergence of paired NRCX/Y specific in Solanaceae
513 species. It is speculated that NRCY might be degenerated from a functional
514 NLR and display a genetically linkage with NRCX after the split between
515 Solanaceae species and Coleophoridae species.

516 *NRCY*-silencing lead to impaired cell death induced by NRC3$^{D480V}$ and
517 Nsm-Sw5b. Furthermore, co-silencing of NRCX and NRCY and NRCY alone
518 consistently both inhibited cell death, suggesting that NRCX regulation of
519 NRC3 function is dependent on NRCY. However, it remains unknown how
520 paired NLRs regulate NRC3-mediated cell death. Many NLRs induce cell
521 death by forming resistosomes. For example, CNLs are activated to form
522 pentamers with cation channels, while TNLs are activated to form tetramers
523 [46-49]. RNLs belong to helper NLR downstream of TNL immunity, which form
524 pentamers in calcium ion channels and finally induce immune responses such
525 as cell death in plants [14]. Recently, NRC2 from NRC-H clade oligomerizes
526 upon effector detection by its sensor NLR [50], indicating that NRC-Hs also
527 form resistosomes. A hypothesis is that NRCX/Y pair might regulate the
528 resistosome-forming process and thus effect the final cell death. It is
529 interesting to determine the mechanism how NRCX/Y regulating the function of
530 NRC-H proteins in the future.

531 Our data expands the current definition of NLR modulators. Two NLR
532 modulators, NRCX and NRG1C are reported and both of them are helper
533 NLRs [30,51]. NRCX belongs to NRC-H family. It contained all NRC-Hs
534 feathers including the MADA motif in N terminal. However, NRCX does not
535 induce cell death but acts as a modulator [30]. Overexpression of NRG1C
536 suppresses autoimmunity of NRG1A, *snc1* and *chs3-2D*, without affecting
537 *chs1*, *chs2* autoimmunity and RPS2-and RPS4-mediated immunity [14].
538 Intriguingly, unlike NRCX, NRG1C is a truncated NLR that lacking the whole
539 N-terminal $CC_R$ domain and is therefore unlikely to execute the hypersensitive

cell death [51]. Here we show that NRCY, which is the conjugated NLR pair of NRCX, is also an NLR modulator. Furthermore, the suppression of NRCX in NRC3 is dependent on NRCY, indicating that NRCX and NRCY are paired NLR modulators.

In eukaryotic genomes, there are approximately 10% of genes are arranged in a head-to-head orientation. These head-to-head orientation often tend to be genes that should be transcribed at equal rates for gene products, suggesting a pattern of shared regulatory regions [52]. For example, co-expression from a head-to-head cluster has been observed for the SOC3–CHS1–TN2 NLR cluster in Arabidopsis, in which the gene products do interact [53,54]. A genome-wide analysis using microarray data for other Arabidopsis head-to-head paired NLRs further supports the co-expression pattern of paired NLRs [53]. In this study, we also observed a common tendency shared by NRCX/Y expressions. In humans, there have even been bidirectional promoters found for paired genes [55]. Although so far no NLRs have been shown to possess bidirectional promoters in plant, it is a potential reason for the co-expression of *NRCX* and *NRCY*. Interestingly, *NRCY* is up-regulated greatly more during leave senescence. We hypothesize that it is probably due to that NRCY is not auto-active and thus releases the selection pressure on restricting *NRCY* transcription during evolution. The mechanism behind should be studied in the future. Additionally, the difference in expression pattern could be used as a clue to identify novel paired NLR modulators.

High immunity level often antagonizes normal plant growth so that age-dependent immunity is a high-efficient strategy for the plant to balance this fitness cost. *N. benthamiana* is reported to have age-dependent resistance against *P. infestans* [25]. Here we showed the difference in resistance between senescent and young leaves on a plant. The senescent leaves are nearly resistant to *P. capsici*, while the young leaves are susceptive (Fig 7C-E). The age-dependent immunity is reported to be related to NLRs in the transcripts level. In *Nicotiana tabacum*, NLRs expression gradually increases

570 with plants matured to form age-dependent immunity [26]. In this study, the
571 expression of *NRCX* and *NRCY* also increased gradually during leaf
572 senescence. Furthermore, the growth rate of *NRCY* expression was higher
573 than that of *NRCX* (Fig 7A). These data combined with the findings that
574 NRCX/Y are paired NLR modulators, together suggested NRCX/Y are
575 involved in age-dependent immunity. In young tissues, where NRCY is less
576 accumulated, it will facilitate plant development, while in mature tissues, highly
577 induced *NRCY* improves plant resistance to pathogens.

578 Collectively, our findings show the negative correlation between paired
579 NLRs and NRC-Hs in Solanaceae species. It highlights a previously neglected
580 co-evolution between NRC-Hs and paired NLRs in Solanaceae species. It also
581 shows the importance of novel role of paired NLRs as modulators in ETI and
582 other biological processes such as in age-dependent immunity.
583

584 # Methods

585 **Identification of NLRs, paired NLRs and NRC-Hs**

586 To identify NLRs, protein sequences from 29 plants were used as input for
587 NLRtracker software [56]. The proteins containing NB-ARC (N) domain
588 predicted by NLRtrack are NLRs. Paired NLRs in all these species were
589 identified based on searching NLRs in a “head-to-head” fashion with enclosing
590 no more than 2 non-NLR genes. Helper NLRs (NRC-Hs) were identified
591 through phylogenetic assay: the NLRs in the same clades with NRC2/3/4 were
592 considered as NRC-Hs.

593 **Growth Conditions of *Nicotiana benthamiana***

594 *N. benthamiana* plants used in this study were grown in the greenhouse at
595 a temperature of 25˚C under a 16-h light/8-h dark photoperiod and 60%
596 relative humidity. The VIGS-treated *N. benthamiana* plants used in this study
597 were grown in a 22˚C greenhouse under a 16-h light/8-h dark photoperiod and
598 60% relative humidity.

599 **Virus-induced gene silencing (VIGS)**

600 VIGS experiments were carried out in *N. benthamiana* as previously
601 described [57]. The binary constructs pTRV2 were transformed into
602 *Agrobacterium* strain GV3101-pMP90. One days before the *Agrobacterium*
603 infiltration, the constructs were incubated at 30°C and 220 rpm for 24 hours.
604 *Agrobacterium* were collected by centrifugation at 4000 rpm for 4 min, washed
605 and re-suspended in infiltration buffer [10 mM $MgCl_2$, 10 mM MES (pH 5.7)
606 and 200 μM acetosyringone], the $OD_{600}$ was adjusted to 0.3. Two-week-old *N.*
607 *benthamiana* plants were infiltrated with a suspension of Agrobacterium
608 carrying TRV RNA1 and TRV RNA2 in a 1:1 ratio.

609 **Transient gene expression and cell death assays**

610 The binary expression plasmids were transferred by electroporation into
611 *Agrobacterium* strain GV3101. Four-weeks old *N. benthamiana* were used for
612 transient expression by *Agrobacterium*. The *Agrobacterium* suspension was
613 configured in the same way as in the VIGS experiment above.
614 To perform RNAi experiments in *N. benthamiana* leaves, *Agrobacterium*
615 carrying RNAi plasmids were injected ($OD_{600}$=0.2) into leaves one day before
616 transient expression of other genes. The $OD_{600}$ of the target gene was
617 adjusted to 0.6. The cell death phenotype was scored and photos were taken
618 7-days post *Agrobacterium* infiltration (dpi). HR scores were modified as from
619 0 (no visible necrosis) to 8 (fully confluent necrosis) (S8C Fig).

620 **Plasmid constructions**

621 All plasmids and primers for the recombinant constructs used in this work
622 are listed in S1 File. NRCX and NRCY was amplified from *N. benthamiana*
623 cDNA and cloned into different vectors such as pCambia1300-3xHA and
624 pCambia1300-3xFlag. Sequences of primers used in cloning of NRCX, NRCY,
625 NRCY variants and NRC3 variants are listed in S1 File. Functional analyses of
626 NRCY and NRC3 were performed with untagged variants, while C-terminally
627 HA or Flag tagged variants showed consistent results with untagged variants
628 in complementation assays.

629 **Measurement of Chorophyll Contents**

630 The chlorophyll content of the fourth true leaf (counted from bottom to top)
631 of each *N. benthamiana* plant was determined using a SPAD Chlorophyll
632 Meter (SPAD-YA, Huoerd). Each leaf was evenly divided into 4 spots, and the
633 average value of the 4 measurements (SPAD Unit) represents a single data
634 point. At least four individual leaves of each treatment are measured, and three
635 biological replicates were performed.

636 **RT-qPCR analysis**

637 Plant total RNA was extracted using an RNA-simple Total RNA Kit
638 (Tiangen Biotech Co., Ltd., Beijing, China). DNA contamination in the RNA
639 sample was removed by 4xgDNA wiper (Vazyme Biotech Co., Ltd., Nanjing,
640 China). 1μg of each RNA sample was subject to first strand cDNA synthesis
641 using the HiScript II Q RT SuperMix for qPCR (Vazyme Biotech Co., Ltd.,
642 Nanjing, China). Real-time PCR was performed on an ABI Prism 7500 Fast
643 Real-Time PCR System using the SYBR Premix Ex Taq kit (Takara Bio Inc.,
644 Shiga, Japan) according to the instructions. Gene expression levels were
645 normalized to the expression of *NbEF1a*, which is stably expressed reference
646 gene in *N. benthamiana*. The primers used in the RT-PCR are listed in S1 File.

647 ***P. capsici* culture conditions *and* inoculation assays**

648 The *P. capsici* strain *LT263* used in this study was cultured and maintained
649 at 25°C in the dark on 10% (v/v) V8 agar plates. The steps of inoculation
650 experiment were as follows: mycelium blocks were placed on the back of the
651 leaves, and 0.1% tween 20 was added at the intersection of mycelium blocks
652 and leaves. After fully moisturizing, the mycelium blocks were placed in a 25°C
653 incubator in darkness for 24 to 36 hours. incubated in an incubator at 25°C for
654 24 to 36 well moisturized and then incubated in a 25°C incubator for 24 to 36
655 hours, photos were taken under ultraviolet light, and the damaged area was
656 measured by Image J software.

657 **Determination of biomass of *Phytophthora capsicum***

658 Diseased leaves of the same quality after inoculation with *Phytophthora*

*capsicum* should be taken, and samples should include all diseased spots. The internal reference genes of *Phytophthora capsicum* and the internal reference genes of *N. benthamiana* were used as the biomass representative genes of *Phytophthora capsicum* and *N.benthaminan* respectively. *T*he biomass of *P. capsicum* in *N. benthamiana* was detected according to the expression levels of these two quantitative reference genes.

**Cultivation of *N. benthamiana* seedlings on 1/2 MS medium**

Put 60 tobacco seeds into a 1.5 mL EP tube, sterilize with 75% ethanol for 30 s, and wash 3 times with sterile water. Then disinfect with 2.5% sodium hypochlorite for 8 minutes and rinse with sterile water 6 times. Seeds were evenly distributed on 1/2 MS medium (0.8% agar powder, pH 5.7). The medium was sealed and placed horizontally at 4 °C for 3 days to break the seed dormancy, then cultured in the greenhouse to wait for the seeds to germinate and grow, and photographed after two or three weeks.

**Protein extraction of *N. benthamiana* leaves**

For normal western blot assay, extraction buffer (50 mM HEPES, 150 mM KCL, 1 mM EDTA, and 0.1% Triton X-100; pH 7.5), supplemented with 1 mM DL-Dithiothreitol (DTT) and protease inhibitor cocktail (Sigma-Aldrich, St. Louis, MO, USA), was used for protein extraction from plant materials. *N. benthamiana* leaves were frozen in liquid nitrogen and polished to a fine powder, add 1ml of the configured protein extract for every 0.5 g of leaves, vortex and mix well, incubate at 4 °C for 30 minutes to fully lyse the sample, centrifuge at 13000 rpm for 15min at 4 °C, take 80 ul of 5 x sample loading buffer, mixed well and then placed in a metal bath at 100 °C for 10min. When the extracted protein is used for Co-IP assay, the above method is used to sample for input in SDS-PAGE, and the remaining supernatant is incubated with target beads.

**Western blot**

Proteins from the sample lysate were fractionated by sodium dodecyl sulfate polyarcylamide gel electrophoresis (SDS-PAGE). Sample in the gel

were transferred to PVDF membrane using eBlot$^{TM}$ L1 (GenScript Corporation). Anti-HA (1:5, 000; #M20013; Abmart Inc., Shanghai, China), anti-flag (1:5, 000; #M20018; Abmart), antibodies were used to bind the protein with the corresponding tag. The total protein is displayed in this paper by ponceau staining.

**Luciferase complementation assay**

The coding sequence of indicated genes was cloned into pCAMBIA1300-35S-HA-Nluc-RBS or pCAMBIA1300-35S-Cluc-RBS and then was transferred into *A. tumefaciens* strain GV3101. The constructs were co-expressed in *N. benthamiana* plants, $OD_{600}$=0.5. The leaves were infiltrated with 1 mM luciferin (Biovision) at 2dpi, then the leaves were detected with a microplate reader (BioTek, Beijing, China). Two leaves were used for each test and three independent experiments were performed with same results.

**Yeast two-hybrid system**

pGBKT7-Bait or pGADT7-Prey constructs used in S9 Fig and were transformed into the yeast strain AH109. Co-transformants were plated on double dropout supplements (SD-LW) and incubated at 28 degrees for 3days. After the yeast colonies on the Double Dropout Supplements plates grew, it indicated that the pGBKT7 and pGADT7 vectors were successfully co-transformed. Next, the yeast colonies were diluted with sterile water to OD600=0.1, followed by another 10-fold and 100-fold, respectively. Take 10 ul of yeast liquid droplets on the double dropout supplements (SD-LW) and triple dropout supplements (SD-LWH), and take pictures and records after incubating at 28 degrees for 3 days.

**Phylogenetic analysis**

Multiple alignments of full-length amino acid sequences were aligned using MUSCLE. Phylogenetic analysis was performed using NB-ARC sequences with the fasttree program [58] or MEGA X program [59] by the maximum likelihood method with 100 bootstrap samples and parameters: poisson model, uniform rates and complete deletion. Alignments data and phylogenetic tree

719 data could be found in S2 and S3 Files.

720 **Accession number**

721 The primary accession codes for PN1a, PN1b, PN2a, PN2b, NRCX,
722 NRCY that support the finding of this study were shown as NbD002668.1
723 (PN1a), NbD002669.1 (PN1b), NbD026701.1 (PN2a), NbD026704.1 (PN2b),
724 NbD022578.1 (NRCY), NbD022579.1 (NRCX), respectively.

725

726 **Abbreviations:**

727 ETI: Effector-triggered immunity; HR: Hypersensitive response; CC:
728 Coiled-coil; TIR: Toll/interleukin 1 receptor (TIR) domain; NRC:NB-ARC:
729 Nucleotide Binding (NB)-ARC (APAF1, R gene products, and CED-4) domain;
730 LRR: Leucine-rich repeat; NRC-H: NRC helper; ID: Integrated decoy; Sensor:
731 An NLR that is responsible for identifying effectors; Helper: Downstream of
732 sensor NLR-mediated immunity; Paired NLR: Two NLR genes, whose loci are
733 very close to each other, work together to regulate immunity; SD Media:
734 Synthetic Dropout Media.

735

# 736 Figure legend

737 **Fig 1. The quantities of paired NLRs and NRC-Hs are negatively**
738 **correlated in Solanaceae species**
739 (A) Summary of predicted NLRs. The phylogeny of the 29 species is based on
740 data from the Taxonomy Database (https://www.ncbi.nlm.nih.gov/taxonomy).
741 The counts of NLRs, paired NLRs and NRCH-s in each species are shown in
742 boxplots following the species names. (B) Scatter plot of %Paired NLRs
743 against %NRC-Hs. Black line represents the linear trend, with dotted line
744 representing the 95% confidence interval. Regression equation (with its R
745 square value) and Person correlation value is shown at top right.
746 **Fig 2. Mutant of *NRCX* is senescence-accelerated, display growth defect**
747 **and high resistance level.**
748 (A) Schematic diagram of six paired NLRs in *N. benthamiana.* (B) The
749 morphology of plants silencing indicated genes. Two-week-old *N. benthamiana*
750 plants were infiltrated with *Agrobacterium* strains carrying tobacco rattle virus
751 (TRV) VIGS constructs, and photographs were taken 4 weeks after
752 agroinfiltration. TRV:*GUS* (*β-glucuronidase*) was used as a negative control.
753 Bar = 2 cm. (C) Schematic diagram showing the deletion of *NRCX* in *N.*

*benthamiana*. The genomic region information of *NRCX* is shown above. The gRNA used for CRISPR/Cas9 editing and DNA sequencing results are shown below. (D) Phenotypes of wild type and *nrcx* knockout mutants grown in soil for 30 days. Bar = 2 cm. (E) Phenotypes of wild type and *nrcx* mutant seedlings on sterile 1/2 MS medium for three weeks. Bar = 1 cm. (F) Chlorophyll content in leaves of *N. benthamiana* wild type and *nrcx* mutant. Asterisks indicate statistically significant differences with t test (mean ± SD, n = 12, $^{**}P < 0.01$), and asterisk in the following text indicates the same meaning. (G,H) Stem length and root length statistics of wild type and *nrcx* grown on 1/2 MS medium for 3 weeks (mean ± SD, n = 7). (I-J) Enhanced resistance in *nrx* mutant. The photos were taken at 24 hours after inoculation (hpi) under UV light. Bar = 2 Inoculated lesion areas are show in (J) (mean ± SD, n = 12). (K) Upregulation of *PR1* expression in *nrcx* mutant. The indicated leaves were inoculated with *P. capsici* for 12 hours and the *PR1* expression was tested (mean ± SEM, n = 3).

**Fig 3. Simultaneously silencing *NRCY* restores the *NRCX*-silenced plants phenotype.**

(A) The morphology of *N. benthamiana* plants silencing indicated genes. TRV:*GUS* was used as a negative control. Two-week-old *N. benthamiana* plants were infiltrated with *Agrobacterium* strains carrying TRV constructs, and the photographs were taken 4 weeks after agroinfiltration. Bar = 2 cm. (B) Leaf diameter of plants silencing indicated genes. The fourth and fifth true leaves (counting from bottom to top) were harvested and the average diameters were recorded. Three independent biological replicates were performed and indicated by different colored dots (n = 16, lowercase letters indicate significant differences tested between multiple groups by one-way ANOVA at $P < 0.05$). (C) Chlorophyll contents of indicated leaves. The fourth true leaf (counting from bottom to top) was taken from five plants silencing indicated genes at 6 weeks of age and the chlorophyll contents were calculated (n = 6, lowercase letters indicate significant differences tested between multiple groups by one-way ANOVA at $P < 0.05$). (D-E) *P. capsici* inoculation phenotypes. Leaves of plants silencing indicated genes were detached and inoculated with *P. capsici* and then incubated in a growth room at 25°C in darkness. Bar = 2 cm. Lesion area was calculated and is shown at (E). Different colored dots indicate different repetitions (n = 37, lowercase letters indicate significant differences tested between multiple groups by one-way ANOVA at $P < 0.05$). (F) Relative *PR1* gene expression levels. The indicated leaves were inoculated with *P. capsici* for 12 hours and the PR1 expression was tested (mean ± SEM, n = 3). (G) Schematic diagram of NRCX and NRCY plant genomes.

**Fig 4. NRCY does not induce HR in *N. benthamiana*.**

(A) P-loop, walker B and MHD motifs of indicated NLRs. The motif sequences of NRC3, NRCX, NRCY and RGA4 are shown. Canonical residues in motifs are marked by blue while non-canonical residues are marked by red. (B) The phenotype of leaves expressing NRCY. GFP and INF1 were used as negative

and positive controls for cell death, respectively. (C) Protein accumulation of NRCY in *N. benthamiana*. Proteins were extracted from leaves at 36 hours after the agroinfiltration. Indicated protein was detected using HA antibody. Total protein loading was confirmed by Ponceau S staining. (D) Cell death induced by the NRC3 mutants. $NRC3^{D480V}$ is an autoactive NRC3 mutant. The phenotypes of leaves expressing NRC3 with walker B motif of NRCY ($NRC3^{EDV}$), NRC3 with MHD motif of NRCY ($NRC3^{LVG}$) and NRC3 with both walker B and MHD motif of NRCY ($NRC3^{EDV+LVG}$) are shown above. Accumulation of the NRC3 variant proteins is shown below. (E) Phenotype of leaves expressing autoactive NRCY mutants. Photos were taken at 5 days post infiltration. (F) Protein accumulation of NRCY autoactive mutants. Total protein loading was confirmed by Ponceau S staining.

**Fig 5. Silencing NRCY impairs Nsm-Sw5b and NRC3-mediated cell death.** (A-D) Hypersensitive response phenotypes in indicated leaves. Photos were taken at 5 days post infiltration and are shown (A,C). Violin plots in (B,D) showing the HR index scored at 5 days post agroinfiltration. Three independent biological replicates were performed and indicated by different colored dot. Asterisks indicate statistically significant differences with *t* test (n > 14, $^{**}P < 0.01$).

**Figure 7. *NRCX* and *NRCY* are involved in age-dependent plant immunity. (A,B) Upregulation of *NRCX* and *NRCY* during leaf senescence.** Leaf positions used to evaluate *NRCX/Y* expressions are labelled in (A). A total of 6 leaves in each positions were sampled for qRT-PCR assay. The relative expression levels of *NRCX* and *NRCY* in leave 1-6 are shown in (B) (mean ± SEM, n = 3). Bar = 2 cm **(C-E) Age-dependent immunity of *N. benthamiana* to *P. capsici*.** Leaves from positions indicated in (A) were sample and inoculated with *P. capsici* mycelium. The photos were taken at 24 hpi (C). Lesion areas were calculated and are shown in (D). Three independent replicates were performed and labelled by different colors (mean ± SD, n > 15, lowercase letters indicate significant differences tested between multiple groups by one-way ANOVA at $P < 0.05$). Relative biomass of *P. capsici* is shown in (E) (mean ± SEM, n = 3, lowercase letters indicate significant differences tested between multiple groups by one-way ANOVA at $P < 0.05$). (F) illustration of working model. The paired NLRs, NRCX/Y, coordinately modulate NRC3-dependent immunity and are involved in age-dependent immunity through different expression level during leave maturation.

# Supporting information

**S1 Fig. The pipeline of paired NLRs and NRC-Hs identification.**
NLR proteins were identified from plant proteome using NLRtracker. Sequences with NB-ARC annotated by NLRtracker were considered as NLRs. NLRs in “head-to-head” fashion with enclosing no more than 2 non-NLR genes are paired NLRs. NRC-Hs were identified by phylogenetic assay (S2 File).

NLR clustered with functionally validated NRC helpers, NRC2/3/4, are NRC-Hs.

**S2 Fig. NLR identification materials and NLR evolutionary trees for different species.**

(A) Summary of plants species used in this study. Different branches of the species are represented by different colors corresponding to figure 1. (B) High similarity between NLR numbers identified in this study and those identified by Ngou et al.. Black line represents the linear trend, with dotted line representing the 95% confidence interval. Regression equation (with its R square value) and Person correlation value is shown at top right.

**S3 Fig. No correlation between %tail-to-tail NLRs and %head-to-head NLRs against %NRC-Hs in Solanaceae species**

(A-B) Scatter plot of %tail-to-tail NLRs and %head-to-head NLRs against %NRC-Hs. Black line represents the linear trend, with dotted line representing the 95% confidence interval. Regression equation (with its R square value) and Person correlation value is shown at top right.

**S4 Fig. Virus-induced silencing of *NRCX* impairs growth and promotes senescence in *N. benthamiana*.**

(A) The silencing efficiency of indicated genes. TRV empty vector (TRV:*GUS*) was used as a negative control. (B) The morphology of 6-week-old *NRCX*-silenced *N. benthamiana* plants. Two-week-old *N. benthamiana* plants were infiltrated with *Agrobacterium* strains carrying tobacco rattle virus (TRV) VIGS constructs, and photographs were taken at 4 weeks after the agroinfiltration. Bar = 2 cm. (C,D) Accelerated senescence in *NRCX*-silenced plants. The fourth true leaf (counting from bottom to top) at 5-week-old plant was harvested (C) and the chlorophyll contents were calculated and shown in (D). Asterisks indicate statistically significant differences with. Three independent biological replicates were performed and indicated by different colored dots (** $P < 0.01$, *t* test; mean ± SD, n =12). Bar = 2 cm. (E) Virus content in TRV:*GUS* and TRV:*NRCX* was detected by qRT-PCR (** $P < 0.01$, *t* test; mean ± SEM, n =12).

**S5 Fig. No off-target effects in *nrcx* mutant.**

(A) Evolutionary tree of *NRCX* homologous genes in *N. benthamiana*. The confidence levels are marked in the node of branches. (B) Flanking sequence of potential CRISPR target. The *nrcx* mutant contains a 7 bp deletion in *NRCX* locus and not mutation could be found in other potential targets.

**S6 Fig. Silencing efficient of *NRCX* and *NRCY* in *N. benthamiana*.**

(A) Gene fragments used for VIGS. The gene fragment used for VIGS are marked by light blue. (B) Silencing efficient of *NRCX* and *NRCY* in VIGS experiments (** $P < 0.01$, *t* test; mean ± SEM, n = 3) (C) Silencing efficient of *NRCX* and *NRCY* in RNAi experiments (* $P < 0.05$, ** $P < 0.01$, *t* test; mean ± SEM, n = 3).

**S7 Fig. The phylogenetic assay of NRCY.**

The maximum likelihood phylogenetic tree was generated in RAxML version 8.2.12 with JTT model using NB-ARC domain sequences of 2189 NLRs identified from tomato (Solyc-), N. benthamiana (NbD-), Coffee (Cc-), Kiwifruit (DTZ-), Sugar beet (EL-), Arabidopsis (AT-), Rice (Os-) (Sl Appendix, FileS3). NRCY-clade and NRCX-clade are marked by blue and orange, respectively. NRCY-clade are expanded and shown below. Domain architecture and motif sequences of NRCY clade members are shown at bottom right. Each motif was identified in MEME using NRCY-clade sequences.

**S8 Fig. NRCX negatively modulates NRC3-mediated cell death.**

(A) Hypersensitive cell death phenotypes. Infiltration site of leaves expressing $NRC3^{D480V}$, $NRC4^{D478V}$, Nsm/Sw5b and Avr3a/R3a were photographed at 5 days post infiltration and related cell death intensities were scored. (B) Calculated HR index of indicated leave sites. Three independent biological replicates were performed and indicated by different colored dot. Asterisks indicate statistically significant differences with *t* test (**$P < 0.01$). (C) The leave phenotype of each HR index. The scale representing cell death extent ranges from 0 (no cell death) to 8 (extensive cell death).

**S9 Fig. CC domains of NRCX and NRCY form heterodimer.**

(A) Schematic diagram of domain segmentation of NRCX and NRCY. (B) Verification of the interaction between CC domains of NRCX and NRCY by yeast two-hybrid (Y2H) assay. Ev/p53 is positive control for interaction. (C) Association between CC domains of NRCX and NRCY detected by luciferase complementation assays. FLS2-nLUC + cLUC-AGB1 was used as positive control.

**S1 File. List of primers in this article.**

**S2 File. NLR evolutionary tree files for 29 species.**

**S3 File. Evolutionary tree file of the gene *NRCY.***

## Declarations

### Ethics approval and consent to participate

Not applicable.

### Consent for publication

Not applicable.

### Availability of data and material

Not applicable.

## Competing interests

The authors declare that they have no competing interests.

## Funding

The work was supported by the National Natural Science Foundation of China (31625023 and 32072507) and the Fundamental Research Funds for the Central Universities (KYT202001 and JCQY201904).

## Authors' contributions

DD, XD and GA conceived and designed the project, jointly performed data analysis and wrote the manuscript. XD, XZ, ZY, JL, CX, WP, TL, HZ, ZY, YZ, YL, ZW, ZK and YY performed the experiments. XD and GA analysed data. DD, XD and GA wrote and modified the manuscript. All authors read and approved the final manuscript.

## Acknowledgements

We appreciate Dr. Min Zhu and Prof. Xiaorong Tao at Nanjing Agricultural University for their gift of NRC3/4 auto-activated mutant, constructive suggestions and help. We appreciate Dr. Meixiang Zhang at Shaanxi Normal University for his help.

# References

1. Ngou BPM, Ding PT, Jones JDG (2022) Thirty years of resistance: Zig-zag through the plant immune system. Plant Cell 34: 1447-1478.
2. Dodds PN, Rathjen JP (2010) Plant immunity: towards an integrated view of plant-pathogen interactions. Nat Rev Genet 11: 539-548.
3. Cui H, Tsuda K, Parker JE (2015) Effector-triggered immunity: from pathogen perception to robust defense. Annu Rev Plant Biol 66: 487-511.
4. Dalio RJD, Paschoal D, Arena GD, Magalhaes DM, Oliveira TS, et al. (2021) Hypersensitive response: From NLR pathogen recognition to cell death response. Annals Of Applied Biology 178: 268-280.
5. Kourelis J, van der Hoorn RAL (2018) Defended to the Nines: 25 Years of Resistance Gene Cloning

954 Identifies Nine Mechanisms for R Protein Function. Plant Cell 30: 285-299.
955 6. Adachi H, Derevnina L, Kamoun S (2019) NLR singletons, pairs, and networks: evolution, assembly,
956 and regulation of the intracellular immunoreceptor circuitry of plants. Curr Opin Plant Biol 50:
957 121-131.
958 7. Griebel T, Maekawa T, Parker JE (2014) NOD-like receptor cooperativity in effector-triggered
959 immunity. Trends Immunol 35: 562-570.
960 8. Eitas TK, Dangl JL (2010) NB-LRR proteins: pairs, pieces, perception, partners, and pathways. Curr
961 Opin Plant Biol 13: 472-477.
962 9. Cesari S, Kanzaki H, Fujiwara T, Bernoux M, Chalvon V, et al. (2014) The NB-LRR proteins RGA4
963 and RGA5 interact functionally and physically to confer disease resistance. EMBO J 33:
964 1941-1959.
965 10. Marchal C, Michalopoulou VA, Zou Z, Cevik V, Sarris PF (2022) Show me your ID: NLR immune
966 receptors with integrated domains in plants. Essays Biochem 66: 527-539.
967 11. Xi Y, Cesari S, Kroj T (2022) Insight into the structure and molecular mode of action of plant
968 paired NLR immune receptors. Essays Biochem 66: 513-526.
969 12. Guo H, Ahn HK, Sklenar J, Huang J, Ma Y, et al. (2020) Phosphorylation-Regulated Activation of
970 the Arabidopsis RRS1-R/RPS4 Immune Receptor Complex Reveals Two Distinct Effector
971 Recognition Mechanisms. Cell Host Microbe 27: 769-781 e766.
972 13. Castel B, Ngou PM, Cevik V, Redkar A, Kim DS, et al. (2019) Diverse NLR immune receptors
973 activate defence via the RPW8-NLR NRG1. New Phytol 222: 966-980.
974 14. Jacob; P, Kim; NH, Wu; F, El-Kasmi; F, Chi; Y, et al. (2021) Plant “helper” immune receptors are
975 Ca2+-permeable nonselective cation channels. Science.
976 15. Wu CH, Derevnina L, Kamoun S (2018) Receptor networks underpin plant immunity. Science 360:
977 1300-1301.
978 16. Wu CH, Abd-El-Haliem A, Bozkurt TO, Belhaj K, Terauchi R, et al. (2017) NLR network
979 mediates immunity to diverse plant pathogens. Proc Natl Acad Sci U S A 114: 8113-8118.
980 17. Zhu M, van Grinsven IL, Kormelink R, Tao X (2019) Paving the Way to Tospovirus Infection:
981 Multilined Interplays with Plant Innate Immunity. Annu Rev Phytopathol 57: 41-62.
982 18. Adachi H, Contreras MP, Harant A, Wu CH, Derevnina L, et al. (2019) An N-terminal motif in
983 NLR immune receptors is functionally conserved across distantly related plant species. Elife
984 8.
985 19. Takken FL, Goverse A (2012) How to build a pathogen detector: structural basis of NB-LRR
986 function. Curr Opin Plant Biol 15: 375-384.
987 20. BIEZEN EAVD, JONES JDG (1998) Plant disease-resistance proteins and the gene-for-gene
988 concept.
989 21. J.Riedl S, Li W, Chao Y, Schwarzenbacher R, Shi Y (2005) Structure of the apoptotic
990 protease-activating factor 1 bound to ADP. Nature 434: 921-926.
991 22. Williams SJ, Sornaraj P, deCourcy-Ireland E, Menz RI, Kobe B, et al. (2011) An Autoactive
992 Mutant of the M Flax Rust Resistance Protein Has a Preference for Binding ATP, Whereas
993 Wild-Type M Protein Binds ADP. MPMI
994 23. van Ooijen G, Mayr G, Kasiem MM, Albrecht M, Cornelissen BJ, et al. (2008) Structure-function
995 analysis of the NB-ARC domain of plant disease resistance proteins. J Exp Bot 59:
996 1383-1397.
997 24. Zou Y, Wang S, Lu D (2020) MiR172b-TOE1/2 module regulates plant innate immunity in an

age-dependent manner. Biochem Biophys Res Commun 531: 503-507.

25. Yusuke Shibata KK, and Daigo Takemoto (2010) Age-Related Resistance of Nicotiana benthamiana Against Hemibiotrophic Pathogen Phytophthora infestans Requires Both Ethylene- and Salicylic Acid–Mediated Signaling Pathways. MPMI.

26. Deng Y, Wang J, Tung J, Liu D, Zhou Y, et al. (2018) A role for small RNA in regulating innate immunity during plant growth. PLoS Pathog 14: e1006756.

27. Ngou BPM, Heal R, Wyler M, Schmid MW, Jones JDG (2022) Concerted expansion and contraction of immune receptor gene repertoires in plant genomes. Nat Plants 8: 1146-1152.

28. Wang L, Zhao L, Zhang X, Zhang Q, Jia Y, et al. (2019) Large-scale identification and functional analysis of NLR genes in blast resistance in the Tetep rice genome sequence. Proc Natl Acad Sci U S A 116: 18479-18487.

29. Wu C-H, Abd-El-Haliem A, Bozkurt TO, Belhaj K, Terauchi R, et al. (2017) NLR network mediates immunity to diverse plant pathogens. Proceedings of the National Academy of Sciences 114: 8113.

30. Adachi H, Sakai T, Harant A, Duggan C, Bozkurt TO, et al. (2021) An atypical NLR protein modulates the NRC immune receptor network. bioRxiv.

31. Karasov TL, Chae E, Herman JJ, Bergelson J (2017) Mechanisms to Mitigate the Trade-Off between Growth and Defense. Plant Cell 29: 666-680.

32. Lozano-Duran R, Zipfel C (2015) Trade-off between growth and immunity: role of brassinosteroids. Trends In Plant Science 20: 12-19.

33. He Z, Webster S, He SY (2022) Growth-defense trade-offs in plants. Curr Biol 32: R634-R639.

34. van Wersch S, Tian L, Hoy R, Li X (2020) Plant NLRs: The Whistleblowers of Plant Immunity. Plant Commun 1: 100016.

35. Tameling WIL, Vossen JH, Albrecht M, Lengauer T, Berden JA, et al. (2006) Mutations in the NB-ARC domain of I-2 that impair ATP hydrolysis cause autoactivation. Plant Physiology 140: 1233-1245.

36. Jubic LM, Saile S, Furzer OJ, El Kasmi F, Dangl JL (2019) Help wanted: helper NLRs and plant immune responses. Curr Opin Plant Biol 50: 82-94.

37. Kanzaki H, Yoshida K, Saitoh H, Fujisaki K, Hirabuchi A, et al. (2012) Arms race co-evolution of Magnaporthe oryzae AVR-Pik and rice Pik genes driven by their physical interactions. Plant J 72: 894-907.

38. De la Concepcion JC, Vega Benjumea J, Bialas A, Terauchi R, Kamoun S, et al. (2021) Functional diversification gave rise to allelic specialization in a rice NLR immune receptor pair. Elife 10.

39. Sarris PF, Duxbury Z, Huh SU, Ma Y, Segonzac C, et al. (2015) A Plant Immune Receptor Detects Pathogen Effectors that Target WRKY Transcription Factors. Cell 161: 1089-1100.

40. Zdrzalek R, Kamoun S, Terauchi R, Saitoh H, Banfield MJ (2020) The rice NLR pair Pikp-1/Pikp-2 initiates cell death through receptor cooperation rather than negative regulation. PLoS One 15: e0238616.

41. Saucet SB, Ma Y, Sarris PF, Furzer OJ, Sohn KH, et al. (2015) Two linked pairs of Arabidopsis TNL resistance genes independently confer recognition of bacterial effector AvrRps4. Nat Commun 6: 6338.

42. Bernoux M, Burdett H, Williams SJ, Zhang X, Chen C, et al. (2016) Comparative Analysis of the Flax Immune Receptors L6 and L7 Suggests an Equilibrium-Based Switch Activation Model. Plant Cell 28: 146-159.

1042 43. Gao Z, Chung EH, Eitas TK, Dangl JL (2011) Plant intracellular innate immune receptor
1043 Resistance to Pseudomonas syringae pv. maculicola 1 (RPM1) is activated at, and functions
1044 on, the plasma membrane. Proc Natl Acad Sci U S A 108: 7619-7624.
1045 44. Wang GF, Ji J, El-Kasmi F, Dangl JL, Johal G, et al. (2015) Molecular and functional analyses of a
1046 maize autoactive NB-LRR protein identify precise structural requirements for activity. PLoS
1047 Pathog 11: e1004674.
1048 45. Wu Z, Li M, Dong OX, Xia S, Liang W, et al. (2019) Differential regulation of TNL-mediated
1049 immune signaling by redundant helper CNLs. New Phytol 222: 938-953.
1050 46. Bi G, Su M, Li N, Liang Y, Dang S, et al. (2021) The ZAR1 resistosome is a calcium-permeable
1051 channel triggering plant immune signaling. Cell 184: 3528-3541 e3512.
1052 47. Wang J, Hu M, Wang J, Qi J, Han Z, et al. (2019) Reconstitution and structure of a plant NLR
1053 resistosome conferring immunity. Science 364.
1054 48. Forderer A, Li E, Lawson AW, Deng YN, Sun Y, et al. (2022) A wheat resistosome defines
1055 common principles of immune receptor channels. Nature 610: 532-539.
1056 49. Ma S, Lapin D, Liu L, Sun Y, Song W, et al. (2020) Direct pathogen-induced assembly of an NLR
1057 immune receptor complex to form a holoenzyme. Science 370.
1058 50. Ahn H-K, Lin X, Olave-Achury AC, Derevnina L, Contreras MP, et al. (2022) Effector-dependent
1059 activation and oligomerization of NRC helper NLRs by Rpi-amr3 and Rpi-amr1. bioRxiv.
1060 51. Wu Z, Tian L, Liu X, Huang W, Zhang Y, et al. (2021) The N-terminally truncated helper NLR
1061 NRG1C antagonizes immunity mediated by its full-length neighbors NRG1A and NRG1B.
1062 Plant Cell.
1063 52. Chen Y, Li Y, Wei J, Li YY (2014) Transcriptional regulation and spatial interactions of
1064 head-to-head genes. BMC Genomics 15: 519.
1065 53. Liang W, van Wersch S, Tong M, Li X (2019) TIR-NB-LRR immune receptor SOC3 pairs with
1066 truncated TIR-NB protein CHS1 or TN2 to monitor the homeostasis of E3 ligase SAUL1.
1067 New Phytol 221: 2054-2066.
1068 54. Liang WW, Tong MXZ, Li X (2020) SUSA2 is an F-box protein required for autoimmunity
1069 mediated by paired NLRs SOC3-CHS1 and SOC3-TN2. Nature Communications 11.
1070 55. van Wersch S, Li X (2019) Stronger When Together: Clustering of Plant NLR Disease resistance
1071 Genes. Trends In Plant Science 24: 688-699.
1072 56. Kourelis J, Sakai T, Adachi H, Kamoun S (2021) RefPlantNLR is a comprehensive collection of
1073 experimentally validated plant disease resistance proteins from the NLR family. PLoS Biol 19:
1074 e3001124.
1075 57. Ratcliff F, Martin-Hernandez AM, Baulcombe DC (2001) Technical Advance. Tobacco rattle virus
1076 as a vector for analysis of gene function by silencing. Plant J 25: 237-245.
1077 58. Price MN, Dehal PS, Arkin AP (2009) FastTree: Computing Large Minimum Evolution Trees with
1078 Profiles instead of a Distance Matrix. Molecular Biology And Evolution 26: 1641-1650.
1079 59. Kumar S, Stecher G, Li M, Knyaz C, Tamura K (2018) MEGA X: Molecular Evolutionary
1080 Genetics Analysis across Computing Platforms. Molecular Biology And Evolution 35:
1081 1547-1549.
1082

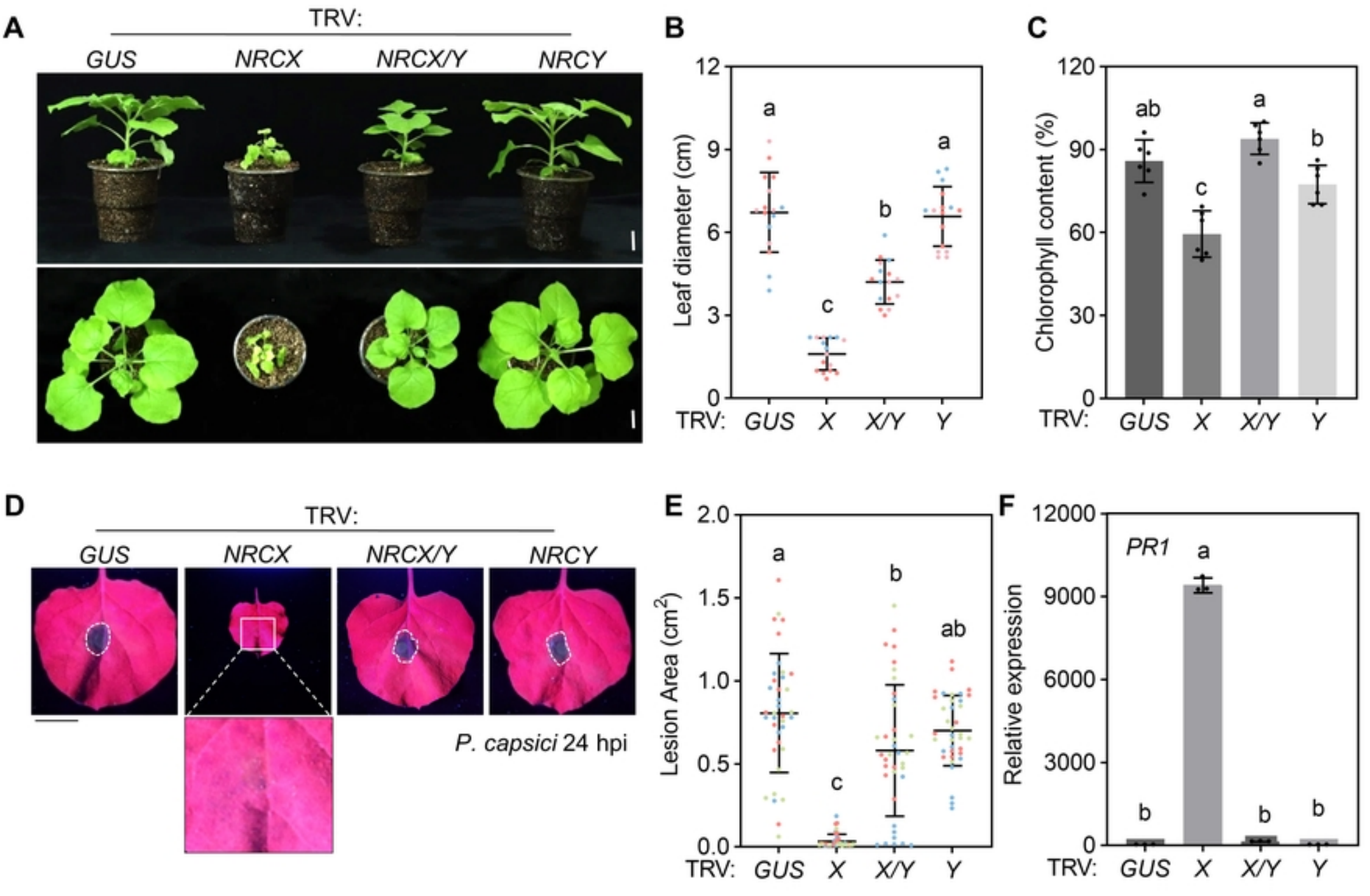
A
TRV:
GUS
NRCX
NRCX/Y
NRCY
B
Leaf diameter (cm)
12
9
6
3
0
a
c
b
a
TRV: GUS X X/Y Y
C
Chlorophyll content (%)
120
90
60
30
0
ab
c
a
b
TRV: GUS X X/Y Y
D
TRV:
GUS
NRCX
NRCX/Y
NRCY
P. capsici 24 hpi
E
Lesion Area (cm2)
2.0
1.5
1.0
0.5
0.0
a
c
b
ab
TRV: GUS X X/Y Y
F
PR1
Relative expression
12000
9000
6000
3000
0
b
a
b
b
TRV: GUS X X/Y Y

Figure 3

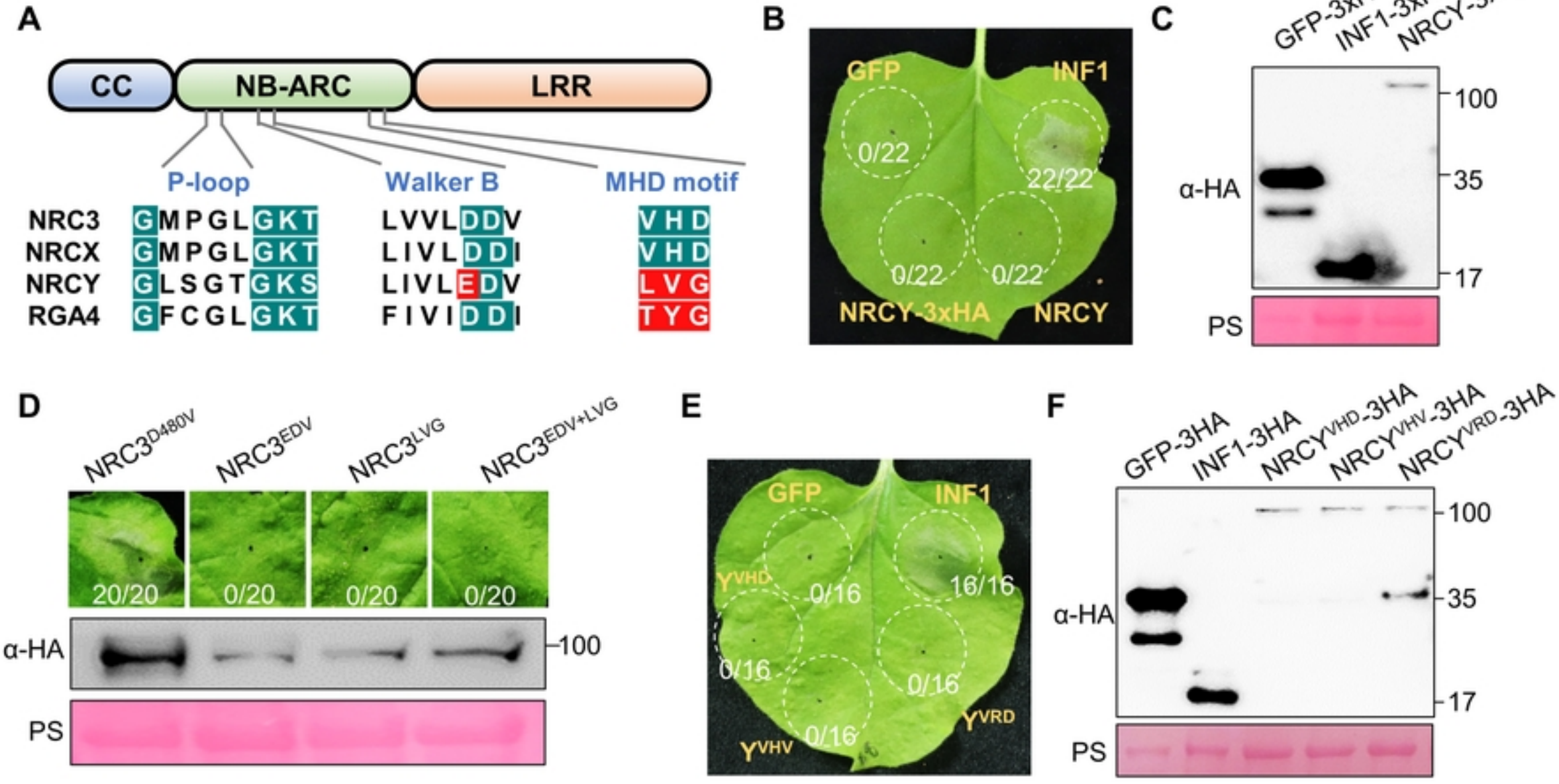
A
CC
NB-ARC
LRR
P-loop
Walker B
MHD motif
NRC3 G M P G L G K T L V V L D D V V H D
NRCX G M P G L G K T L I V L D D I V H D
NRCY G L S G T G K S L I V L E D V L V G
RGA4 G F C G L G K T F I V I D D I T Y G
B
GFP
INF1
0/22
22/22
0/22
0/22
NRCY-3xHA
NRCY
C
GFP-3xHA
INF1-3xHA
NRCY-3xHA
α-HA
100
35
17
PS
D
NRC3D480V
NRC3EDV
NRC3LVG
NRC3EDV+LVG
20/20
0/20
0/20
0/20
α-HA
100
PS
E
GFP
INF1
YVHD
0/16
16/16
0/16
0/16
0/16
YVRD
YVHV
F
GFP-3HA
INF1-3HA
NRCYVHD-3HA
NRCYVHV-3HA
NRCYVRD-3HA
α-HA
100
35
17
PS

Figure 4

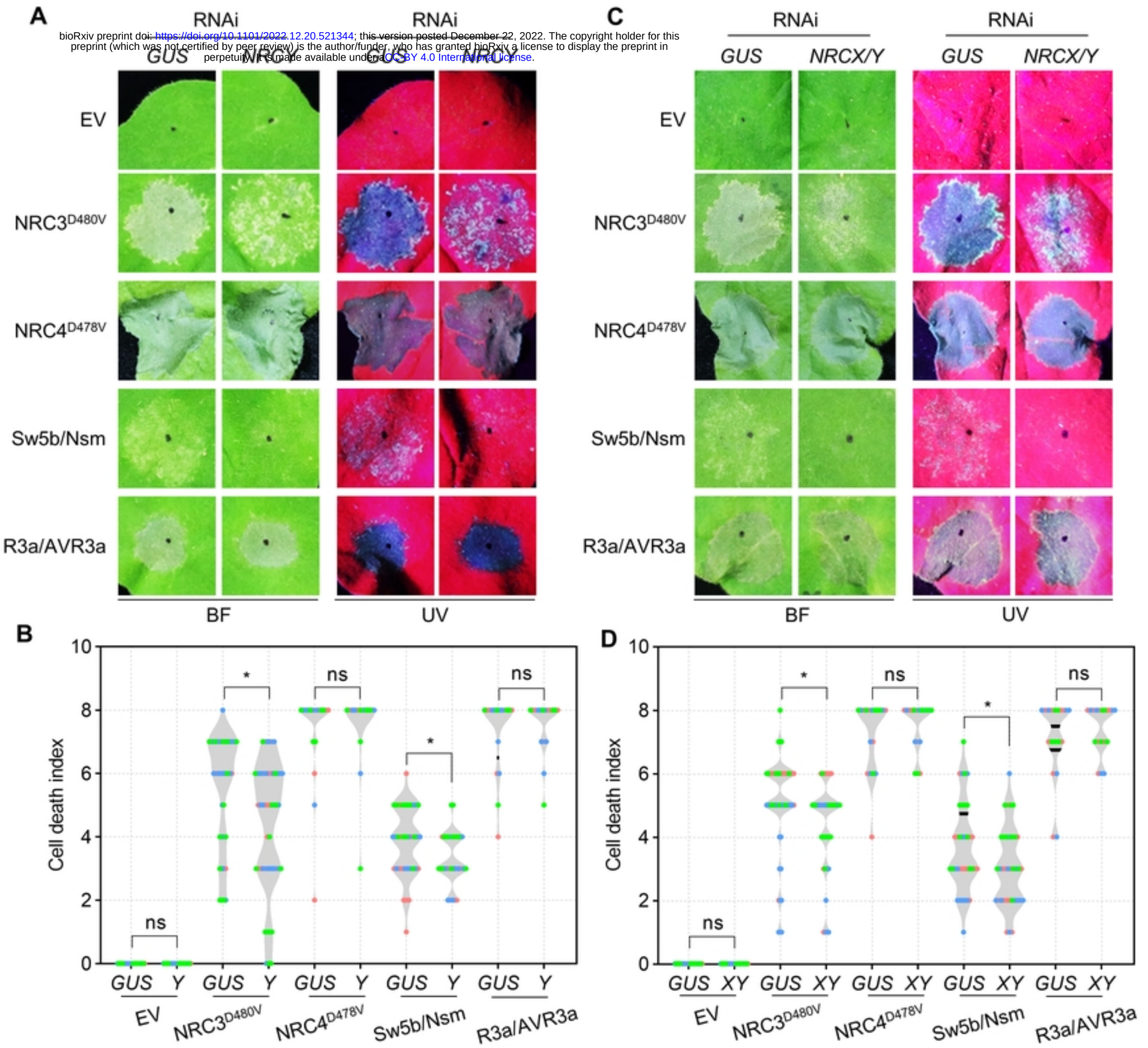


Figure 5

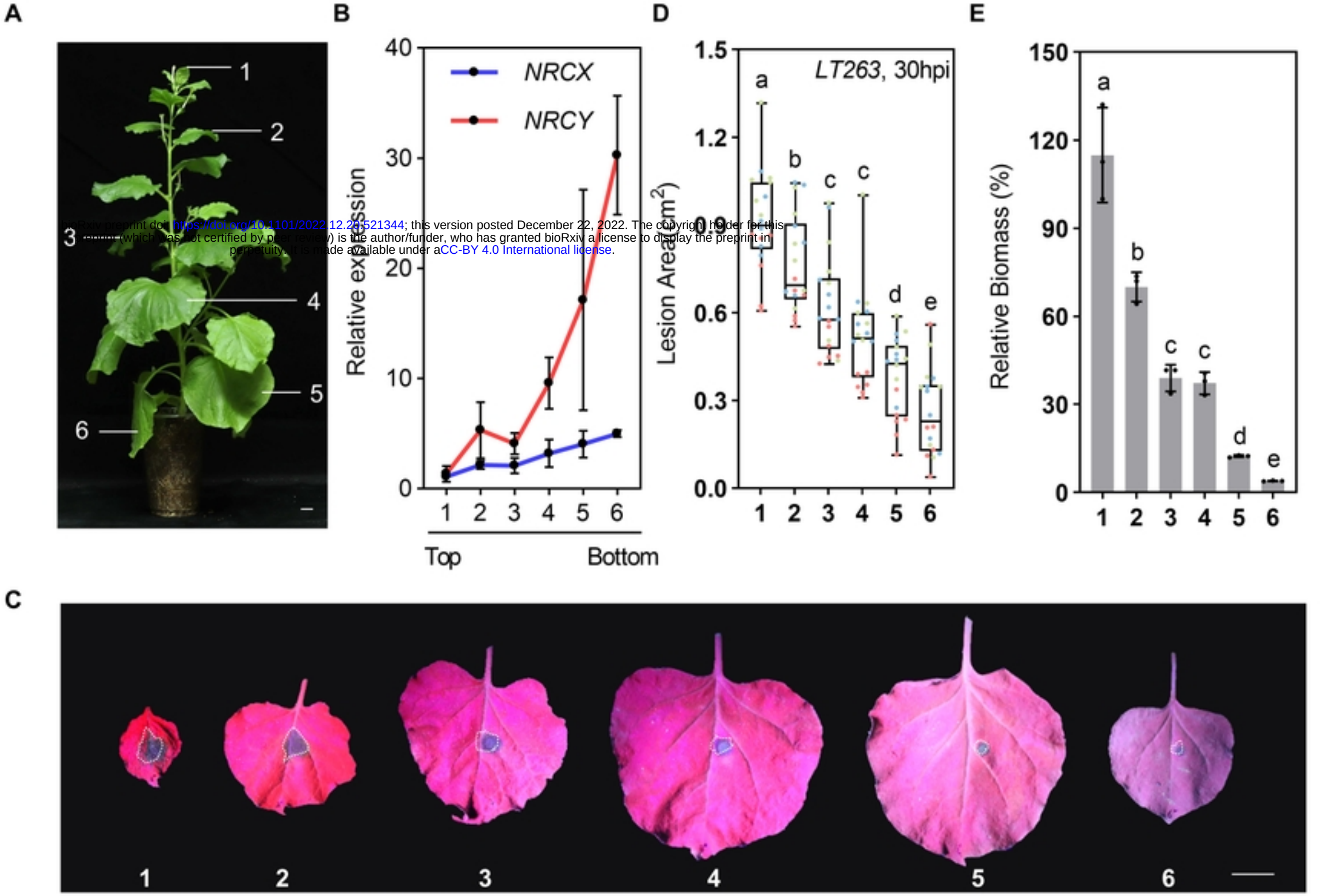


Figure 6

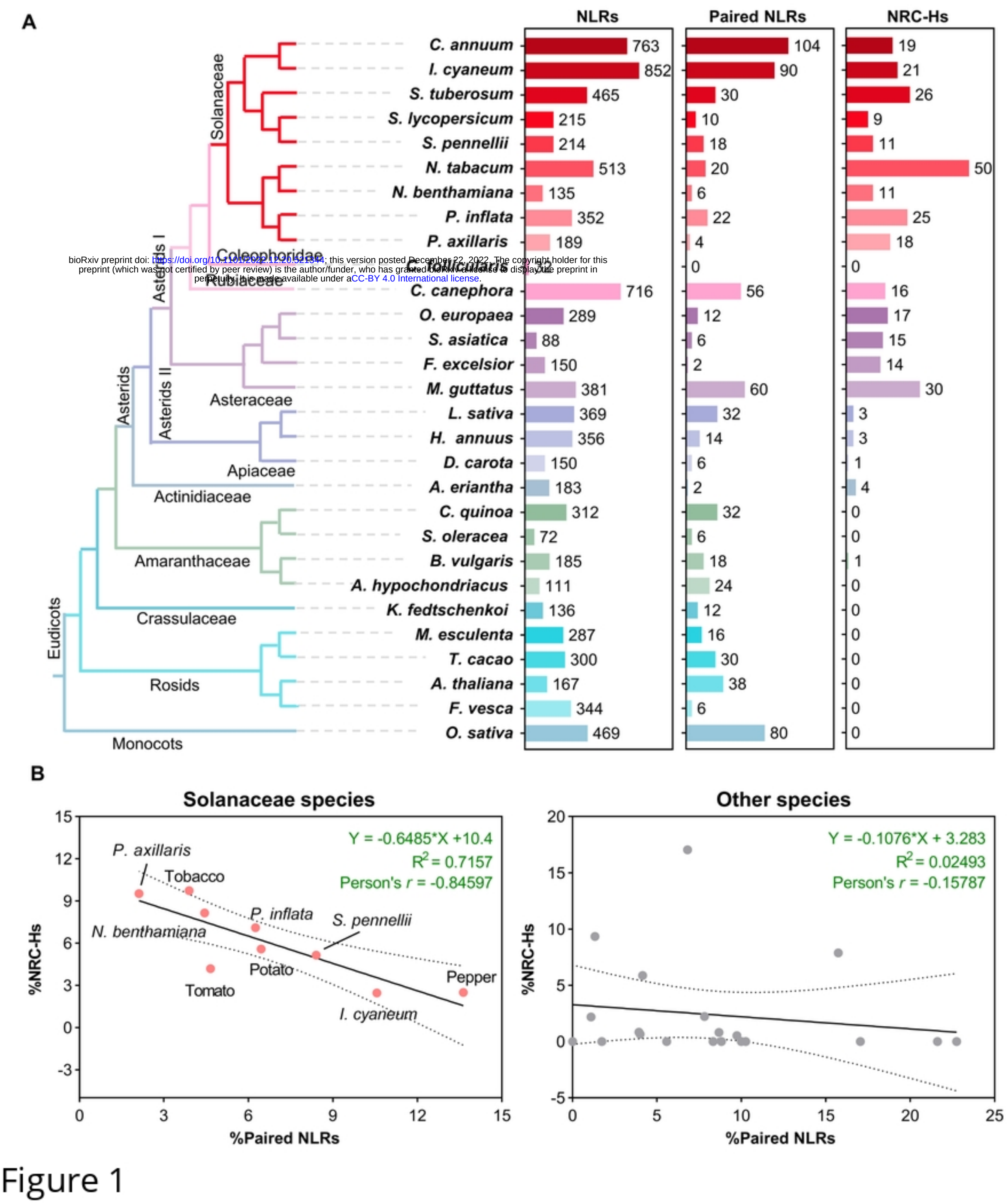


Figure 1

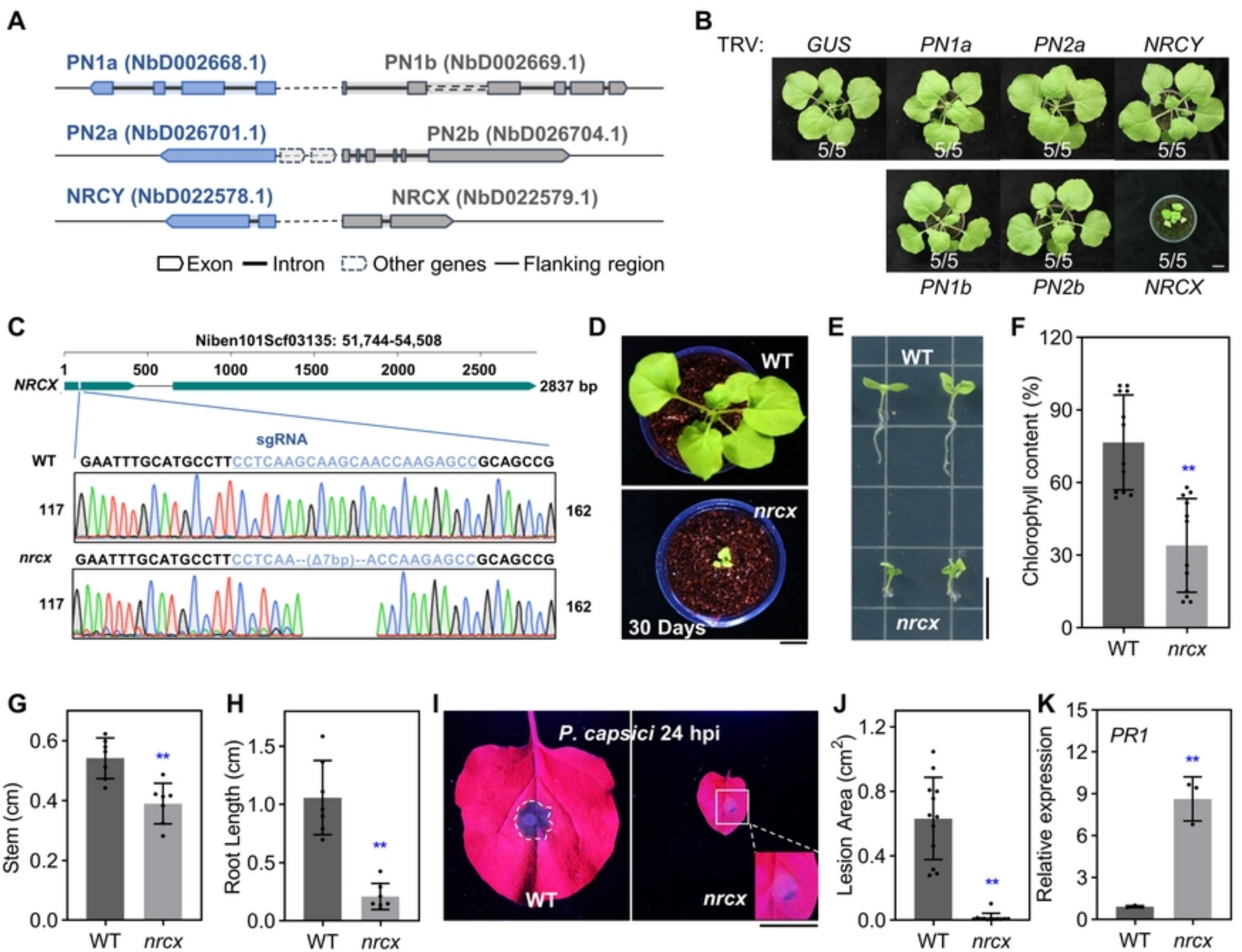
A
PN1a (NbD002668.1)
PN1b (NbD002669.1)
PN2a (NbD026701.1)
PN2b (NbD026704.1)
NRCY (NbD022578.1)
NRCX (NbD022579.1)
Exon
Intron
Other genes
Flanking region
B
TRV:
GUS
PN1a
PN2a
NRCY
5/5
PN1b
PN2b
NRCX
C
Niben101Scf03135: 51,744-54,508
NRCX
2837 bp
sgRNA
WT
GAATTTGCATGCCTTCCTCAAGCAAGCAACCAAGAGCCGCAGCCG
nrcx
GAATTTGCATGCCTTCCTCAA--(Δ7bp)--ACCAAGAGCCGCAGCCG
117
162
D
WT
nrcx
30 Days
E
WT
nrcx
F
Chlorophyll content (%)
WT
nrcx
G
Stem (cm)
H
Root Length (cm)
I
P. capsici 24 hpi
J
Lesion Area (cm²)
K
PR1
Relative expression

Figure 2